Journal of Orthopaedic Translation 48 (2024) 89–106

Contents lists available at ScienceDirect

Journal of Orthopaedic Translation

journal homepage: www.journals.elsevier.com/journal-of-orthopaedic-translation

Original Article

Exosomes derived from bone marrow mesenchymal stem cell preconditioned by low-intensity pulsed ultrasound stimulation promote bone–tendon interface fibrocartilage regeneration and ameliorate rotator cuff fatty infiltration

Bing Wu [a,b,c,d], Tao Zhang [a,b,c,d], Huabin Chen [a,b,c,d], Xin Shi [a,b,c,d], Changbiao Guan [a,b,c,d], Jianzhong Hu [d,e,f,**], Hongbin Lu [a,b,c,d,*]

[a] Department of Sports Medicine, Xiangya Hospital, Central South University, Changsha, 410008, Hunan, China
[b] Key Laboratory of Organ Injury, Aging and Regenerative Medicine of Hunan Province, Changsha, 410008, Hunan, China
[c] Hunan Engineering Research Center of Sports and Health, Changsha, 410008, China
[d] National Clinical Research Center for Geriatric Disorders, Xiangya Hospital, Central South University, Changsha, 410008, Hunan Province, China
[e] Department of Orthopedics, Xiangya Hospital, Central South University, Changsha, 410008, Hunan, China
[f] Mobile Health Ministry of Education - China Mobile Joint Laboratory, Changsha, 410008, Hunan Province, China

ARTICLE INFO

Keywords:
Bone-tendon insertion
Exosomes
Low-intensity pulsed ultrasound stimulation (LIPUS)
Mesenchymal stem cells
Rotator cuff

ABSTRACT

Background: Fibrovascular scar healing of bone-tendon interface (BTI) instead of functional fibrocartilage regeneration is the main concern associated with unsatisfactory prognosis in rotator cuff repair. Mesenchymal stem cells (MSCs) exosomes have been reported to be a new promising cell-free approach for rotator cuff healing. Whereas, controversies abound in whether exosomes of native MSCs alone can effectively induce chondrogenesis.

Purpose: To explore the effect of exosomes derived from low-intensity pulsed ultrasound stimulation (LIPUS)-preconditioned bone marrow mesenchymal stem cells (LIPUS-BMSC-Exos) or un-preconditioned BMSCs (BMSC-Exos) on rotator cuff healing and the underlying mechanism.

Methods: C57BL/6 mice underwent unilateral supraspinatus tendon detachment and repair were randomly assigned to saline, BMSCs-Exos or LIPUS-BMSC-Exos injection therapy. Histological, immunofluorescent and biomechanical tests were detected to investigate the effect of exosomes injection on BTI healing and muscle fatty infiltration of the repaired rotator cuff. *In vitro*, native BMSCs were incubated with BMSC-Exos or LIPUS-BMSC-Exos and then chondrogenic/adipogenic differentiation were observed. Further, quantitative real-time polymerase chain reaction (qRT-PCR) was performed to detect the chondrogenesis/adipogenesis-related miRNA profiles of LIPUS-BMSC-Exos and BMSC-Exos. The chondrogenic/adipogenic potential of the key miRNA was verified through function recover test with its mimic and inhibitor.

Results: The results indicated that the biomechanical properties of the supraspinatus tendon-humeral junction were significantly improved in the LIPUS-BMSC-Exos group than that of the BMSCs-Exos group. The LIPUS-BMSC-Exos group also exhibited a higher histological score and more newly regenerated fibrocartilage at the repair site at postoperative 2 and 4 weeks and less fatty infiltration at 4 weeks than the BMSCs-Exos group. *In vitro*, co-culture of BMSCs with LIPUS-BMSC-Exos could significantly promote BMSCs chondrogenic differentiation and inhibit adipogenic differentiation. Subsequently, qRT-PCR revealed significantly higher enrichment of chondrogenic miRNAs and less enrichment of adipogenic miRNAs in LIPUS-BMSC-Exos compared with BMSC-Exos. Moreover, we demonstrated that this chondrogenesis-inducing potential was primarily attributed to miR-140, one of the most abundant miRNAs in LIPUS-BMSC-Exos.

Conclusion: LIPUS-preconditioned BMSC-Exos can effectively promote BTI fibrocartilage regeneration and ameliorate supraspinatus fatty infiltration by positive regulation of pro-chondrogenesis and anti-adipogenesis, which was primarily through delivering miR-140.

* Corresponding author. Department of Sports Medicine, Xiangya Hospital, Central South University, Changsha, 410008, Hunan, China.
** Corresponding author. Department of Orthopedics, Xiangya Hospital, Central South University, Changsha, 410008, Hunan, China.
E-mail addresses: jianzhonghu@csu.edu.cn (J. Hu), hongbinlu@csu.edu.cn (H. Lu).

https://doi.org/10.1016/j.jot.2024.07.009
Received 14 September 2023; Received in revised form 28 May 2024; Accepted 18 July 2024
2214-031X/© 2024 The Authors. Published by Elsevier B.V. on behalf of Chinese Speaking Orthopaedic Society. This is an open access article under the CC BY-NC-ND license (http://creativecommons.org/licenses/by-nc-nd/4.0/).

The translational potential of this article: These findings propose an innovative "LIPUS combined Exosomes strategy" for rotator cuff healing which combines both physiotherapeutic and biotherapeutic advantages. This strategy possesses a good translational potential as a local injection of LIPUS preconditioned BMSC-derived Exos during operation can be not only efficient for promoting fibrocartilage regeneration and ameliorating rotator cuff fatty infiltration, but also time-saving, simple and convenient for patients.

What is known about this subject

MSC-Exos could enhance tendon-bone healing and ameliorate the development of fatty infiltration after rotator cuff reconstruction. Biological functions of the generated Exos were determined by the state of the Exos donor cells. Whether LIPUS treatment reinforce biological function of MSC-Exos, especially pro-chondrogenesis (promote fibrocartilage regeneration) and anti-adipogenesis (reduce fatty infiltration) properties, remain unclear. Meanwhile, the specific components of MSC-Exos that perform these functions are still unknown.

What this study adds to existing knowledge

LIPUS precondition of BMSCs effectively amplify the pro-chondrogenesis and anti-adipogenesis bioactivity of BMSCs-Exos, which contribute to more fibrocartilage regeneration at BTI and less fatty infiltration in rotator cuff muscle. Moreover, the chondrogenesis-inducing potential was primarily attributed to miR-140, one of the most abundant miRNAs in LIPUS-treated MSCs-Exos.

1. Introduction

Tendon integrates with bone through a specialized fibrocartilaginous tissue [1]. The bone-tendon insertion (BTI) plays a critical role in mediating load transmission and minimizing concentrated stress between tendon and bone [2–4]. Surgical reconstruction are standard treatments for rotator cuff injuries, with over 270,000 shoulder rotator cuff repairs performed annually in the United States alone [5]. However, surgical repair is simply a physical re-attachment of tendon to bone and valid evidence demonstrates that BTI healing occurs through formation of disorganized fibrovascular scar tissue with high levels of type III collagen rather than regeneration of a ordered transitional fibrocartilaginous tissue that consists of high levels of collagen type II and proteoglycans [6–9], which means the fibrocartilage layer is regenerated slowly and incompletely at the BTI. Therefore, achievement of BTI healing, specifically fibrocartilage regeneration at the BTI is the key for a successful clinical outcome [10–12]. Meanwhile, fatty infiltration of the repaired supraspinatus is another adverse factor that impair the function of the repaired rotator cuff [13,14]. After rotator cuff tendon injury, the rotator cuff muscles undergo characteristic degenerative changes, including fatty infiltration and muscle atrophy [15–17]. Many studies have demonstrated that fatty infiltration progressed over time after surgical repair of massive rotator cuff tears, although a intact repair slowed down the rate of progression [15,18–20]. Gladstone et al. [19] reported a rotator cuff retear rate of 67%–70 % in patients with moderate to severe fatty infiltration and 22%–29 % in those with no or mild fatty infiltration. Additionally, advanced fatty infiltration is closely associated with poor clinical outcome after rotator cuff repair [18,19,21–23]. Hence, it is also important to alleviate or halt fatty infiltration after the repair of rotator cuff tears [24,25].

Exosomes (Exos) released from mesenchymal stem cells (MSCs) can exert biological activities similar to those of the MSCs by transferring information to damaged tissue [26]. MSCs can regulate the differentiation of other neighboring stem cells, such as osteogenesis, adipogenesis and angiogenesis [27–29]. However, there's a lot of controversy as to whether the Exos of native MSCs can effectively induce chondrogenesis [28,30–32]. Actually, few literature demonstrate that the Exos of native MSCs alone can effectively induce chondrogenesis. In recent years, increasing evidence indicates that the biological functions of the generated Exos were determined by the state of the Exos donor cells [33]. Most recently, Exos derived from Kartogenin preconditioned human umbilical cord mesenchymal stem cells (hUCMSCs) were proven to be able to promote chondrogenesis of native hUCMSCs [28]. Besides, it was found that small extracellular vesicles (sEVs) derived from miR-92a-3p-overexpressing BMSCs could facilitate cartilage proliferation and suppress cartilage degradation [32]. All these studies indicate a promising prospect that Exos released from specially treated MSCs can trigger the stable lineage-specific chondrogenic differentiation of native MSCs [28].

LIPUS is an established, widely applied and Food and the Drug Administration (FDA) approved intervention for enhancing bone healing in fractures and non-unions [34]. LIPUS is a classical nondestructive biophysical therapy in which mechanical energy is transmitted transcutaneously as high-frequency acoustical pressure waves into biological tissues [35]. Over the last two decades, LIPUS therapy has been proved to be an effective strategy to enhance repair of articular cartilage and stimulate tendon-bone junction healing [35–43]. Meanwhile, LIPUS can induce chondrogenesis of BMSCs *in vitro* by enhancing the synthesis of matrix proteins such as collagen type II and proteoglycans and expression of chondrogenic markers such as *Sox9* and *TIMP-2* [44]. However, whether LIPUS achive its chondrogenic function through paracrine factors, especially Exos, remain unclear. All these data provide us with valuable sight of LIPUS preconditioning of MSCs-derived Exos as a promising new cell-free biotherapy agent to trigger the chondrogenesis of MSCs in cartilage repair. To the best of our knowledge, there was no previous study report MSCs Exos derived from LIPUS intervention.

In present research, we investigated the feasibility of applying Exos derived from LIPUS preconditioned BMSCs (LIPUS-BMSC-Exos) as a novel biomimetic tool to promote fibrocartilage regeneration and alleviate fatty infiltration in a murine rotator cuff repair model. We also assessed the effects of LIPUS-BMSC-Exos on chondrogenesis and adipogenesis *in vitro* and preliminarily clarified the underlying mechanism.

2. Materials and methods

2.1. Study design

In vivo study: All animal protocols were approved by the Animal Committee of Central South University (No. 2019030490). The sample size was decided according to previously published data demonstrated that at least six specimens were needed for biomechanical testing and four for histologic analysis in the murine rotator cuff injury model (effect size of 70 %, $\alpha = 00.05$, and power of 0.80) [45,46]. A total of 120 mature (12-week-old, average weight: 25 g) male C57BL/6 mice underwent unilateral supraspinatus tendon (ST) detachment and repair procedure following rodent animal model of rotator cuff tear [45]. The mice were randomly allocated to one of the three groups according to different treatments: Control group ($n = 40$), BMSC-Exos group ($n = 40$), and LIPUS- BMSC-Exos group ($n = 40$), which intervened with saline, BMSCs-Exos or LIPUS-BMSC-Exos injection, respectively (Fig. S1). Animals were housed in cages and allowed to free cage activity after surgery. Mice were euthanized at postoperative week 2 and 4 to harvest the supraspinatus muscle-supraspinatus tendon-humeral (SMSTH) complex for tests. Eight specimens from each group at each time point were used for biomechanical testing (failure load and stiffness), six specimens were evaluated by histological testing (mean cell density, bone-to-tendon

insertion maturing score, fibrocartilage area and thickness, and integrated optical density of proteoglycan), while the other six specimens were evaluated by immunofluorescence staining (mean fluorescence intensity of Scleraxis, SOX9 and Collagen type II). The order of all treatments and measurements at the same stage of experiments for the mice is random. The outcome measurements were performed in a blinded fashion by two independent raters. All data analyses were performed by the same person in the investigational team (B.W.).

In vitro study: Native BMSCs were co-cultured with LIPUS-BMSC-Exos, BMSC-Exos, blank liposome, miRNA mimic and miRNA inhibitor. Then, chondrogenic and adipogenic differentiation assays were performed (n = 6 per group) (Fig. S2). Chondrogenesis of different groups were quantitatively compared using the Bern score and the mRNA expression of chondrogenic-related gene of *Sox9*, *Aggrecan*, *Col2a1*. Adipogenesis were quantitatively assessed by intensity of oil red staining of mature adipocytes, and the mRNA expression of adiponectin (*Adipo*), resistin (*Retn*) and peroxisome proliferator-activated receptor-gamma (*Pparg*).

2.2. Isolation and identification of BMSCs

Six 4-week-old mice were euthanized and their femurs and tibias were obtained immediately. Bone marrows were flushed out from marrow cavity and were blew evenly. Suspensions were incubated with standard media comprising α-MEM (Gibco, Grand Island, USA) supplemented with 10 % fetal bovine serum (FBS; Gibco), 100 U/mL penicillin and 100 μg/mL streptomycin (Gibco) at 37 °C in a humidified atmosphere of 5 % CO2 and 95 % air. The medium was replaced after colonies of fibroblast-like cells appeared. After 3–4 days of incubation (at 80 % confluence), cells were re-plated in 10-cm Petri dishes. Early-passage BMSCs (passage 3–4) were used for the follow-up experiments.

An inverted microscope (Leica DMI6000B, Solms, Germany) was used to observe the morphology of BMSCs. Immunophenotype of BMSCs was identified by flow cytometry with the characteristic surface markers of multipotential stem cells (CD29, CD34, CD44, CD45, and CD90). All antibodies were purchased from BD Biosciences (San Jose, USA). The adipogenic, osteogenic and chondrogenic differentiation potentials of BMSCs were determined by using the respective differentiation medium (Cyagen Biosciences Inc, Guangzhou, China). Adipogenesis of BMSCs was evaluated using Oil Red O (ORO) staining to observe lipid droplets at day 21 of induction, osteogenesis of BMSCs was examined using Alizarin Red S (ARS) staining to test calcium depositions at day 14 of induction, and chondrocyte differentiation of BMSCs was assessed by Toluidine Blue staining of extracellular matrix at day 21 of induction.

2.3. LIPUS intervention of BMSCs

An ST-SONIC LIPUS exposure apparatus from ITO Corporation Ltd. was used (Tokyo, Japan) to apply LIPUS intervention on BMSCs. BMSCs at passage 3 were cultured in six-well plates. When cells grew to about 80 % confluence, the culture medium was replaced by an Exos-depleted FBS-containing medium (EXO-FBS-250A-1; System Biosciences, Mountain View, USA). After BMSCs reached confluence, the dish was put on the transducer of the LIPUS apparatus which located at the cell incubator. The cells were exposed to LIPUS from the bottom of the culture dish with a coupling gel placed between the LIPUS transducer and culture dish. The distance between the transducer and the cells was approximately 5–6 mm. The ultrasound exposure was conducted for 20 min daily at a frequency of 1.5 MHz in a pulsed-wave mode (200 μs pulse burst width with repetitive frequency of 1 kHz at the intensity of 30 mW/cm^2) [47,48].

2.4. Exos Extraction and labeling

After received LIPUS treatment or natural culture (also cultured in Exos-depleted FBS-containing medium) for 3 days, the conditioned medium was collected and sequentially centrifuged at 300×*g* for 10min, 2000×*g* for 30 min, 10,000×*g* for 30 min and then filtered through a 0.22 mm filter (BD Biosciences) to eliminate dead cells and cellular debris. The supernatant was then subjected to ultracentrifugation at 100,000×*g* for 4 h at 4 °C. After washing with PBS (100,000×*g* for 20 min), the Exos-containing pellet was resuspended in a right amount of PBS. The protein concentration of the Exos suspension was quantified by BCA protein assay kit (Thermo Fisher Scientific, Waltham, USA). Exos were stored at −80 °C for later use. The morphology of Exos was observed by transmission electron microscope (Hitachi, Tokyo, Japan). Exos particle size distribution and particle number were determined by Nanoparticle tracking analysis (NTA) using ZetaView PMX 120 (Particle Metrix, Inning am Ammersee, Germany). The expression of specific surface markers (CD9, CD63, Calnexin and TSG101) was identified by Western Blot assay.

To track the location and internalization of the Exos, they were pre-stained with DiR stains (40757ES25, Yeasen, Shanghai, China) for *in vivo* study and with PKH26 green fluorescent cell linker kit (Sigma–Aldrich, St. Louis, USA) for *in vitro* study according to the manufacturer's instructions. After labeling, the Exos were washed in PBS and collected by ultracentrifugation (100,000×*g* for 30 min) at 4 °C. Then, the labeled Exos were resuspended in serum-free α-MEM as previously described [49].

2.5. Animal model and Exos treatment

The mice underwent unilateral ST detachment and repair in the left shoulder according to previous protocols [46,50,51]. In brief, after anesthetized with intraperitoneal injection of 0.3 % pentobarbital sodium (0.6 mL/20 g; Sigma–Aldrich), a longitudinal incision was made on the lateral side of the left shoulder. The deltoid muscle was then minimally detached at the surgical neck of humerus. External rotation of left shoulder was made and the acromion was elevated to adequately expose the supraspinatus tendon-humeral. A 6-0 PROLENE™ polypropylene suture needle (Double armed; Ethicon, San Lorenzo, USA) was sutured through ST in an "8" figure fashion. Then, the ST was sharply transected at its insertion site on the greater tuberosity, and the remaining tendon and fibrocartilage layer of the footprint were gently abraded with a No.15 blade to expose the bellowing spongy bone. A 30-gauge needle was used to carefully drill a transosseous bone tunnel traversing the humeral head under the footprint. Finally, the ST was tied to its original insertion site with the two suture limbs shuttled through the tunnel, one from the interior to the lateral, and the other from the lateral to the interior [51].

After repair, BMSC-Exos or LIPUS-BMSC-Exos (10^{11} Exos suspended in 20 μL of PBS [52]) were injected at ST and supraspinatus muscle (SM). The mice in the control group were injected with an equal volume of saline at the time of repair. After injection, the wounds were closed in layers. All the mice were allowed free cage activity after surgery.

2.6. Exos tracking in vivo

To track the DiR labeled Exos *in vivo*, a non-invasive *in vivo* fluorescence tracking system (IVIS Spectrum, PerkinElmer, USA) was used to image the DiR signal distribution and intensity on the mice shoulder at 3 days and 7 days post-operation.

2.7. Histological and immunofluorescent analyses

The SMSTH complex specimens were harvested from left shoulder joint at postoperative 2, 4 and 8 weeks and divided into two parts: the SM and the supraspinatus tendon-humeral (STH) complex. The STH samples were fixed in 4 % paraformaldehyde for 24 h and then decalcified in ethylene diamine tetraacetic acid(EDTA) decalcifying fluid (Servicebio, Wuhan, China) for 7 days. The SM specimens were routinely fixed in GD solution for 24 h.

STH samples at postoperative 2 and 4 weeks were used for histological analysis. STH specimens were fixed, decalcified and embedded in paraffin, 5 μm-thick sections from the mid–coronal plane of each specimen, which through the supraspinatus tendon and the greater tuberosity, were sliced by a microtome (Leica RM2125; Reichert-Jung GmbH). The STH sections were stained with hematoxylin and eosin (H&E, Solarbio Co Ltd, Beijing, China) and toluidine blue O/fast green (TB&FG, Sigma–Aldrich). The SM specimens at postoperative 4 and 8 weeks were embedded in optimal cutting temperature compound (OCT, Sakura finetec USA inc, Torrance, USA) and then 5 μm-thick frozen transverse sections of SM myofibers were obtained. The SM sections were stained with ORO (Solarbio Co Ltd). H&E Sections were used for histological description of the repaired BTI junction, and semi-quantitative analysis for cell density around the BTI [53]. Toluidine blue O/fast green stained slices were used to calculate the area, thickness [54], and proteoglycan content [41,55] of the regenerated fibrocartilage layer using ImageJ software (Version 1.32, National Institutes of Health; Bethesda, MD, USA). A modified bone-to-tendon maturing score adapted from Ide et al. [56] which includes cellularity, vascularity, continuity, fibrocartilage cells, and tidemark and ranks on a scale from 1 to 4 (Table S1) was applied to evaluate healing and maturation of the tendon repair site on H&E and TB&FG staining images. All sections were observed using a transmitted light microscope (Olympus CX31; Olympus Inc, Hamburg, Germany) under the same conditions. To assay the area percentage of fatty infiltration, images of the entire cross-section of ORO-stained SM were scanned with a digital slide scanner (Pannoramic MIDI; 3DHISTECH Ltd, Budapest, Hungary) and then measured by ImageJ software (National Institutes of Health) for quantification.

For immunofluorescence staining for fibrocartilage-related markers of Scleraxis (SCX), SRY (sex determining region Y)-box 9 (SOX9) and Collagen II, the STH specimens were embedded in optimal cutting temperature compound (OCT, Sakura finetec USA inc, Torrance, USA) and then 5 μm-thick frozen sections were acquired. After washed out for OCT and blocked with 3 % BSA at room temperature for 30 min, The frozen sections were incubated with the primary antibody SCX (1:200; Abcam, Cambridge, Britain), Collagen II (1:100; Affinity Biosciences, Changzhou, China) and SOX9 (1:200; Abcam) overnight at 4 °C. After washing three times with PBS, sections were incubated with the secondary antibody (1:1000; Abcam) at room temperature for 2 h in a dark environment. Nuclei were stained with DAPI (0.5 μg/mL; Invitrogen). The signals were examined with a Zeiss Axio Imager M2 fluorescence microscope (Zeiss, Solms, Germany) equipped with an Apotome.2 System. Mean fluorescence intensity (MFI) determination was made using ImageJ software and the MFI values were normalized to 100 cells [57].

2.8. Biomechanical testing

For biomechanical testing, each STH complex was carefully dissected from surrounding tissues under a surgical microscope and stored at −80 °C immediately. The specimens were thawed at room temperature before testing and were keep moist in 0.9 % saline solution at 37 °C during the test. Biomechanical testing was conducted with investigators blinded to groups. Before testing, all sutures in STH complex were confirmed to be carefully removed. The humerus was mounted and the supraspinatus tendon was secured in a clamp using sandpaper. The STH complex was placed into a microcomputer controlled electronic material testing system (WD-T, Zhuoji Instrument Equipment Co., Ltd. Shanghai, China) which allow a uniaxial tensile at an abduction angle of approximately 60°. The specimens were preconditioned under a preload between 0 N and 0.5 N for 3 times and then loaded to failure at a rate of 1 mm/min. The failure load was recorded, and the stiffness was calculated as the slope of the best-fit line on the linear region of the force–displacement curve on the software (MATLAB, Natick, USA) according to the methods proposed by Stephen et al. [58].

2.9. miRNA transfection

The native BMSCs were cultured in 12-well plate until reaching 90 % confluency. Then, 500 μl of transfection mix (Lipofectamine 3000; Invitrogen) with 200 nM miR-140 mimic, mimic negative control (mimic NC), miR-140 inhibitor or inhibitor negative control (inhibitor NC) (RiboBio, China) was added into the culture medium respectively and incubated at 37 °C for 6 h [59]. Transfection efficiencies of mimic and inhibitor were confirmed by qRT-PCR.

2.10. Exos uptake assay in vitro

To observe Exos internalization by BMSCs, native BMSCs were incubated with serum-free α-MEM containing LIPUS-BMSC-Exos or BMSC-Exos at a final concentration of 20 μg/mL for 6 and 12 h [60]. Then, cells were stained with CytoPainter Phalloidin-iFluor 488 reagent (ab176753, abcam, Cambridge, MA) for 30 min and washed with PBS. Nuclei were stained with DAPI (0.5 μg/mL; Invitrogen, Carlsbad, USA). The cellular uptake of Exos was examined by Zeiss Axio Imager M2 microscope. To determine the uptake of Exos-derived miRNAs, BMSCs cells were treated with Exos for 12 h and then collected to analyze the expression of miRNAs by qRT-PCR.

2.11. Chondrogenic differentiation assay

The 3D pellet culture [28] was performed to induce chondrogenic differentiation of BMSCs. In brief, native BMSCs were incubated with 1 mL of growth medium containing 20 μg/mL blank liposomes, BMSC-Exos, LIPUS-BMSC-Exos [28,49,60]. BMSCs transfected with miR-140 mimic or mimic NC were cultured in 1 mL of growth medium, while BMSCs transfected with miR-140 inhibitor or inhibitor NC were cultured in 1 mL of growth medium containing 20 μg/mL of LIPUS-BMSC-Exos components [28]. After 48 h culture, a suspension containing 5×10^5 cells were collected into a 15 mL centrifuge tube, centrifuged to form pellets and cultured in growth medium. The medium was replaced every 3 days for all groups. 3 weeks later, the pellets were fixed, embedded in paraffin, sectioned, and stained with H&E, Toluidine blue, and Safranine O. Chondrogenesis of different groups were quantitatively compared using the Bern score system [61]. Briefly, the higher total score means the better degree of neocartilage formation. The levels of chondrogenesis-specific marker of collagen II (1:100, 4 °C overnight) were assessed by immunohistochemistry in different groups. Briefly, the pellets were fixed, sectioned, stained, counterstained, dehydrated, hyalinized, and mounted. What's more, the expression of chondrogenic-related gene of *Sox9*, *Aggrecan*, *Col2a1* was analyzed by qRT-PCR.

2.12. Adipogenic differentiation assay

For adipogenic differentiation assays, native BMSCs, mimic or inhibitor transfected BMSCs (5×10^5 cells per well) were plated in 12-well culture plates and cultured until reaching confluence. Then, adipogenesis induction medium (Cyagen Biosciences) were used to induce adipogenic differentiation following the manufacturer's protocol supplemented with LIPUS-BMSC-Exos, BMSC-Exos or liposomes (20 μg/mL). After 7 days of induction, the expression of *Adipo*, *Retn* and *Pparg* mRNA was analyzed by qRT-PCR. After 3 weeks, the cells were stained with ORO to detect mature adipocytes.

2.13. qRT-PCR analysis

For miRNA detection, total Exos-derived miRNAs were isolated using the miRNeasy Micro Kit (Qiagen, Hilden, Germany). Then the Mir-X™ miRNA First-Strand Synthesis Kit (Takara Biotechnology, Shiga, Japan) were used to synthesize cDNA for miRNAs according to the manufacturer's protocol. Amplification reactions were performed using a miRNA

SYBR Green qRT-PCR Kit (Takara) with the provided universal reverse primer and miRNA reference gene U6. The miRNA-specific forward primers were synthesized by RiboBio (Guangzhou, China).

For mRNA analysis, total RNA from cultured cells was extracted using Trizol Reagent (Invitrogen). cDNA was synthesized from 1 μg total RNA by using a Revert Aid First-strand cDNA Synthesis Kit (Fermentas, Life Sciences, Canada). Then, amplification reactions were performed with FastStart Universal SYBR Premix ExTaqTMII (Takara Biotechnology) in an ABI PRISM® 7900HT System (Applied Biosystems, Foster City, USA). Relative mRNA expression was calculated by the relative standard curve method (2-△△CT) with GAPDH as the reference. The PCR primers used in this study were as follows: *Col2a1*: forward, 5′-CAGGATGCCCGAAAATTAGGG3′, and reverse, 5′-ACCACGATCACCTCTGGGT3’; *Sox9*: forward, 5′-CGGAACAGACTCACATCTCTCC3′, and reverse, 5′-GCTTGCACGTCGGTTTTGG3’; *Aggrecan*: forward, 5′-CCTGCTACTTCATCGACCCC3′, and reverse, 5′-AGATGCTGTTGACTCGAACCT3’; *Adipo:* forward, 5′-GATGGCAGAGATGGCACTCC-3′, and reverse, 5′-CTTGCCAGTGCTGCCGTCAT-3’; *Retn*: forward, 5′-TTGCTGGACAGTCTCCTCCAGAGGG-3′, and reverse, 5′-AAGCGACCTGCAGCTTACAGCAG-3’; *Pparg*: forward, 5′-TGTCTCATAATGCCATCAGGTTTG-3′, and reverse, 5′-GATAACG. AATGGTGATTTGTCTGTT-3’.

2.14. Western Blot analysis

Total proteins of Exos were extracted using RIPA lysis buffer supplemented with a protease inhibitor (Sigma). Extracted proteins were subjected to sodium dodecyl sulfate-polyacrylamide gel electrophoresis (SDS-PAGE) separation and then transferred onto polyvinylidene fluoride membranes (Millipore, Darmstadt, Germany). After blocking with 5 % non-fat milk for 2 h, the membranes were incubated with primary antibodies overnight at 4 °C. Then, the membranes were washed and incubated with horseradish peroxidase-conjugated secondary antibodies for 1 h at room temperature. The immunoreactive bands were visualized using a chemiluminescence reagent (Thermo) and imaged by the ChemiDoc XRS Plus luminescent image analyser (Bio-Rad, Hercules, USA). Primary antibodies were used in this study as follows: anti-CD9 (1:500; BD), anti-CD63 (1:500; BD), anti-TSG101 (1:1000; ProteinTech, Chicago, USA), anti-Calnexin (1:500, Abcam).

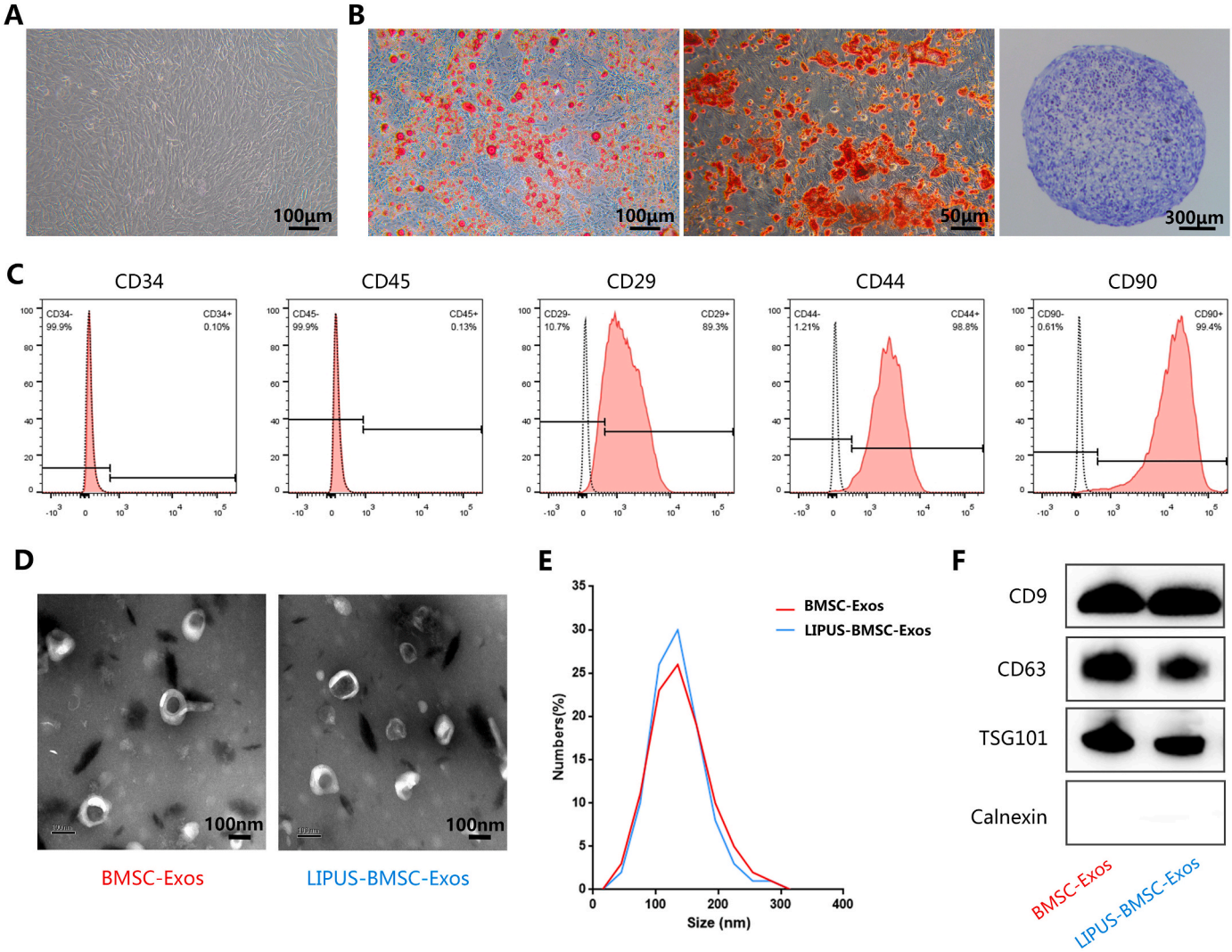

Fig. 1. Characterization of BMSCs and BMSCs-derived exosomes. (A) BMSCs demonstrated a spindle fibroblast-like morphology. **(B)** BMSCs were capable of differentiating into adipocytes, osteoblasts or chondrocytes after adipogenic, osteogenic or chondrogenic medium induction, indicated by Oil Red O (ORO) staining, Alizarin Red S (ARS) staining and Alcian Blue staining. **(C)** Flow cytometry analysis of the typical surface markers in BMSCs. Blank curves: the unlabeled BMSCs controls; solid red curves: the test samples. **(D)** Morphology of bone marrow mesenchymal stem cell-derived exosomes (BMSC-Exos) and bone marrow mesenchymal stem cell-derived exosomes induced by LIPUS (LIPUS-BMSC-Exos) under transmission electron microscopy. **(E)** Size distribution of Exos calculated by Nanoparticle tracking analysis. **(F)** Detection of the Exos surface markers (CD9, CD63, TSG101 and Calnexin) in BMSC-Exos and LIPUS-BMSC-Exos by Western Blot.

2.15. Statistical analysis

Data are shown as means ± standard deviation (SD). Student's t test was used to analyze differences between two groups. Data were confirmed normal distribution by the Kolmogorov–Smirnov normality test before analysis of variance (ANOVA) analysis. For multiple group comparisons, two-way ANOVA was utilized, and Tukey's multiple comparisons test was used to analyze significant differences between groups. If the homogeneity of variance test shows significance, the Welch ANOVA were used to perform multiple group comparisons. Statistical analysis was conducted using GraphPad Prism software (Version 8, San Diego, USA) and $P < 0.05$ was considered statistically significant.

3. Results

3.1. Characterization of BMSCs and BMSCs derived Exos

BMSCs isolated from mice bone marrow exhibited a typical spindle fibroblast-like morphology under light microscopy (Fig. 1A) and were able to differentiate into adipocytes, osteoblasts or chondrocytes after adipogenic, osteogenic or chondrogenic medium induction (Fig. 1B). Flow cytometric analysis showed that BMSCs were positive for CD29, CD44, and CD90, and negative for CD34 and CD45 (Fig. 1C). The Exos (BMSC-Exos and LIPUS-BMSC-Exos) we obtained presented a typical cup-like appearance with double membrane structures ranging from 50 to 200 nm under transmission electron microscope (Fig. 1D), and the NTA indicated that the size distributions of BMSC-Exos and LIPUS-BMSC-Exos are homogeneous (Fig. 1E). No obvious difference of particles numbers was detected between the two groups ($P > 0.05$). Furthermore, Western Blot analysis demonstrated that these nanovesicles expressed exosomal marker proteins including CD9, CD63, and TSG101 and were negative for Calnexin (Fig. 1F). The data indicated that these nanoparticles are Exos.

3.2. Exosomes tracking in vivo

After injection of DiR labeled BMSC-Exos or LIPUS-BMSC-Exos at SMSTH complex for 3 and 7 days, the non-invasive tracking system (IVIS Spectrum) was used to image the DiR distribution and intensity. IVIS images showed that positive DiR signal was detected on the mice shoulder in the BMSC-Exos group and the LIPUS-BMSC-Exos group, which were proved to exist at SMSTH complexes by the lateral view of the SMSTH tissues (Fig. 2A). Quantification analysis found no significant difference of fluorescence intensity between the 2 groups at day 7 ($P = 0.947$, Fig. 2B). The data suggested that the labeled Exos were delivered to the targeted area.

3.3. LIPUS-BMSC-Exos enhance BTI healing by promoting regeneration of fibrocartilage zone

For H&E staining, supraspinatus tendon (ST) was healed to the humeral head and the enthesis was gradually regenerated with time. At

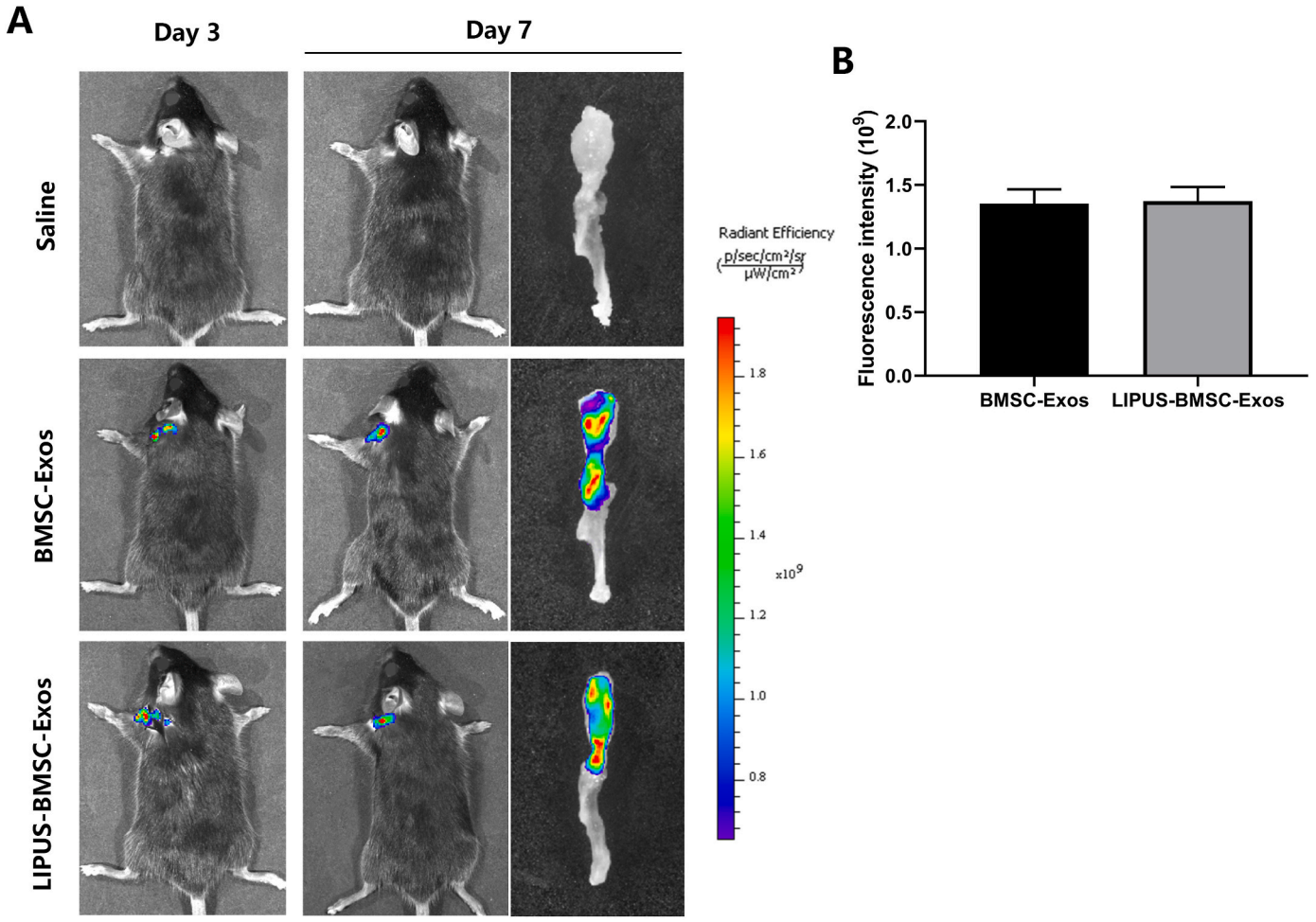

Fig. 2. Tracking of the injected exosomes. (A) A non-invasive *in vivo* fluorescence tracking analysis and immunofluorescent staining demonstrated that DiR-labeled Exos were delivered to the targeted area (SMSTH complex). **(B)** Quantification analysis showed no significant difference of fluorescence intensity between the BMSC-Exos group and LIPUS-BMSC-Exos group. Scale bar: 100 μm.

postoperative 2 weeks, fibrovascular tissue was found at the BTI which was poorly organized with abundant inflammatory cells and some cartilage-like cells (Fig. 3A). The mean cell density in the BTI was lower in the LIPUS-BMSC-Exos groups (4744 ± 401 cells/mm^2) compared with the BMSC-Exos group (6058 ± 526 cells/mm^2) and the control group (6117 ± 555 cells/mm^2) ($P < 0.05$ for both, Fig. 3C). At postoperative 4 weeks, BTI regeneration and remolding were observed in the attachment, which was distinguished with prevalent fibrocartilage cells characterized with inconspicuous nucleus and larger cartilage lacuna than those chondroid cells appeared at week 2 (Fig. 3A). Mean cell density in the BTI was lower in both the LIPUS-BMSC-Exos group (3884 ± 386 cells/mm^2) and the BMSC-Exos group (4429 ± 425 cells/mm^2) compared with the control group (5853 ± 604 cells/mm^2) ($P < 0.01$ for both). In addition, the mean cell density in the BMSC-Exos group was still significantly higher than that in the LIPUS-BMSC-Exos group ($P < 0.01$, Fig. 3C).

For Toluidine blue O/fast green staining, fibrovascular tissue was found at the BTI interface, without obvious gaps in all groups at postoperative 2 weeks. At postoperative 4 weeks, varying degrees of hypertrophic fibrocartilage-like cells embedded by a characteristic matrix rich in proteoglycans were observed in all groups (Fig. 3B). Obvious more fibrocartilage formation was noted in the LIPUS-BMSC-Exos group at both postoperative 2 and 4 weeks. Quantitatively, the area, thickness, proteoglycan content of fibrocartilage layer and the modified bone-to-tendon maturing score in the LIPUS-BMSC-Exos group were significantly higher than those of the other 2 groups at both postoperative 2 and 4 weeks ($P < 0.05$ for all, Fig. 3D and E). Additionally, the BMSC-Exos group showed more regenerated fibrocartilage than the control group at postoperative 4 weeks ($P < 0.05$ for all), while there was no significant difference between the 2 groups at postoperative 2 weeks ($P > 0.05$ for all, Fig. 3D and E).

Immunofluorescence staining showed that the LIPUS-BMSC-Exos group exhibited significantly higher mean fluorescence intensity (MFI) value of SCX, SOX9 and Collagen II (Fig. 4) compared to the BMSC-Exos group and the saline group at postoperative 4 weeks ($P < 0.001$ for all). Compared with the saline group, the BMSC-Exos group still showed significantly higher MFI value of fibrocartilage-related markers expression ($P < 0.001$, Fig. 4D-F).

3.4. LIPUS-BMSC-Exos decrease fatty infiltration of the repaired rotator cuff

Fatty infiltration of supraspinatus increased progressively with time and obvious fatty infiltration could be seen in the saline group at postoperative 4 weeks (Fig. 5A). At week 4, the LIPUS-BMSC-Exos group showed significantly lower fatty infiltration (9.33 % ± 1.10 %) compared with the BMSC-Exos group (13.59 % ± 1.21 %) and the saline group (19.22 % ± 2.02 %) ($P < 0.001$ for both, Fig. 5B). At week 8, The degree of fat infiltration obviously increased in the saline group and slightly increased in the LIPUS-BMSC-Exos group and the BMSC-Exos group (Fig. 5A). Quantitatively, fatty infiltration area in the LIPUS-BMSC-Exos group (9.51 % ± 1.08 %) was significantly lower than that of the BMSC-Exos group (14.50 % ± 1.19 %) and the saline group (26.52 % ± 3.1 %). These findings indicate that local injection of LIPUS-BMSC-Exos into the BTI at the time of repair showed marked inhibition of supraspinatus fatty infiltration.

3.5. LIPUS-BMSC-Exos enhance biomechanical properties of the repaired rotator cuff

In biomechanical test, all STH complexes failed at the tendon-bone attachment. Intact normal STH enthesis were tested and used as a reference to evaluate healing status of the three groups (failure load, 5.21 ± 0.16 N and stiffness, 3.80 ± 0.06 N/mm). The mean ultimate load to failure of the LIPUS-BMSC-Exos group at postoperative 4 weeks (4.68 ± 0.17 N) and at postoperative 8 weeks (5.02 ± 0.18 N) were significantly greater than that in the control group (3.52 ± 0.20 N at 4 weeks, 3.54 ± 0.22 N at 8 weeks, respectively) and in the BMSC-Exos group (4.13 ± 0.14 N at 4 weeks, 4.19 ± 0.14 N at 8 weeks, respectively) ($P < 0.001$ for all, Fig. 5E). Meanwhile, stiffness was also significantly greater in the LIPUS-BMSC-Exos group than in the control group and the BMSC-Exos group at both postoperative 4 and 8 weeks ($P < 0.01$ for all, Fig. 5D and E). Obvious difference of the failure load and stiffness between the BMSC-Exos group and the control group were also noted at postoperative 4 weeks ($P < 0.01$ for stiffness and $P < 0.001$ for failure load) and 8 weeks ($P < 0.01$ for both, Fig. 5D and E).

3.6. Detection of miRNAs in LIPUS-BMSC-Exos

To explore the key molecules that mediate the therapeutic potential of LIPUS-BMSC-Exos on promoting BTI fibrocartilage regeneration and ameliorating fatty infiltration, qRT-PCR analysis was used to detect the levels of a class of miRNAs in LIPUS-BMSC-Exos, including miR-127-5p, miR-455-3p, miR-381-3p, miR-365, miR-8485, miR-675-5p, miR-320c, miR-526b-3p, miR-337-3p, miR-140, miR-181b-3p, miR-3131, miR-181a-3p, miR-5690, miR-1263, miR-27a, miR-27b-3p, miR-24, miR-304-5p, miR-379-5p, miR-503-5p, which have been reported to promote chondrogenesis [62–64], and miR-17, miR-204-5p, miR-21, miR-148a, miR-143, miR-483-5p, miR-204, miR-125-3p, miR-205, miR-20a-5p, miR-214-5p, which have been reported to promote adipogenesis [63]. The data revealed that miRNA cargoes in the LIPUS-BMSC-Exos group were indeed different from the BMSC-Exos cargoes (Fig. 6A and B). In detail, 14 out of 21 chondrogenetic miRNAs, including miR-127-5p, miR-381-3p, miR-365, miR-675-5p, miR-526b-3p, miR-337-3p, miR-140, miR-181b-3p, miR-3131, miR-27a, miR-27b-3p, miR-379-5p and miR-503-5p, were significantly upregulated in the LIPUS-BMSC-Exos group ($P < 0.01$ for all, Fig. 6A). Whereas 7 out of 11 adipogenetic miRNAs, including miR-21, miR-148a, miR-143, miR-483-5p, miR-205, miR-20a-5p, miR-17 were significantly downregulated compared with the BMSC-Exos group ($P < 0.01$ for all, Fig. 6B). Among the 14 upregulated miRNAs in LIPUS-BMSC-Exos, the concentration of miR-140 was much higher compared with other miRNAs (Fig. 6A). Thus, we focused on LIPUS-BMSC-Exos-derived miR-140 for further investigation.

3.7. LIUPUS-BMSC-Exos deliver miR-140 into BMSCs

To detect whether LIUPUS-BMSC-Exos or BMSC-Exos could be taken up by native BMSCs *in vitro*, Exos labeled with PKH26 dye (red fluorescence) were incubated with native BMSCs for 6 and 12 h. As shown in Fig. 6C, the PKH26-labeled Exos were found in the cytoplasm of native BMSCs. We next determined the transfer of miR-140 into recipient cells. After treatment with LIUPUS-BMSC-Exos or BMSC-Exos for 12 h, BMSCs cells were harvested for miR-140 detection. qRT-PCR analysis demonstrated that miR-140 levels in native BMSCs were remarkably increased after incubation with LIUPUS-BMSC-Exos compared with those incubated with BMSC-Exos ($P < 0.001$, Fig. 6D). The results suggest that miR-140 can be shuttled into target cells by LIUPUS-BMSC-Exos.

3.8. LIPUS-BMSC-Exos promote chondrogenic differentiation of BMSCs

After incubation with different Exos components, recipient cells were subjected to pellet culture, and chondrogenesis was evaluated by histological examination and qRT-PCR 21 days later. Cartilage lacuna-like structures and extracellular matrix deposition were observed in the LIPUS-BMSC-Exos group (Fig. 7A), whereas no obvious chondrogenesis was observed in the Blank group and the BMSC-Exos group. In addition, the Bern score and expression of chondrogenesis-related genes (*Sox9*, *Aggrecan*, and *Col2a1*) in the LIPUS-BMSC-Exos group were remarkably elevated compared with the BMSC-Exos group and the blank group ($P < 0.01$ for all, Fig. 7B-E). Notably, the BMSC-Exos group showed no significant difference of Bern score and expression of chondrogenesis-

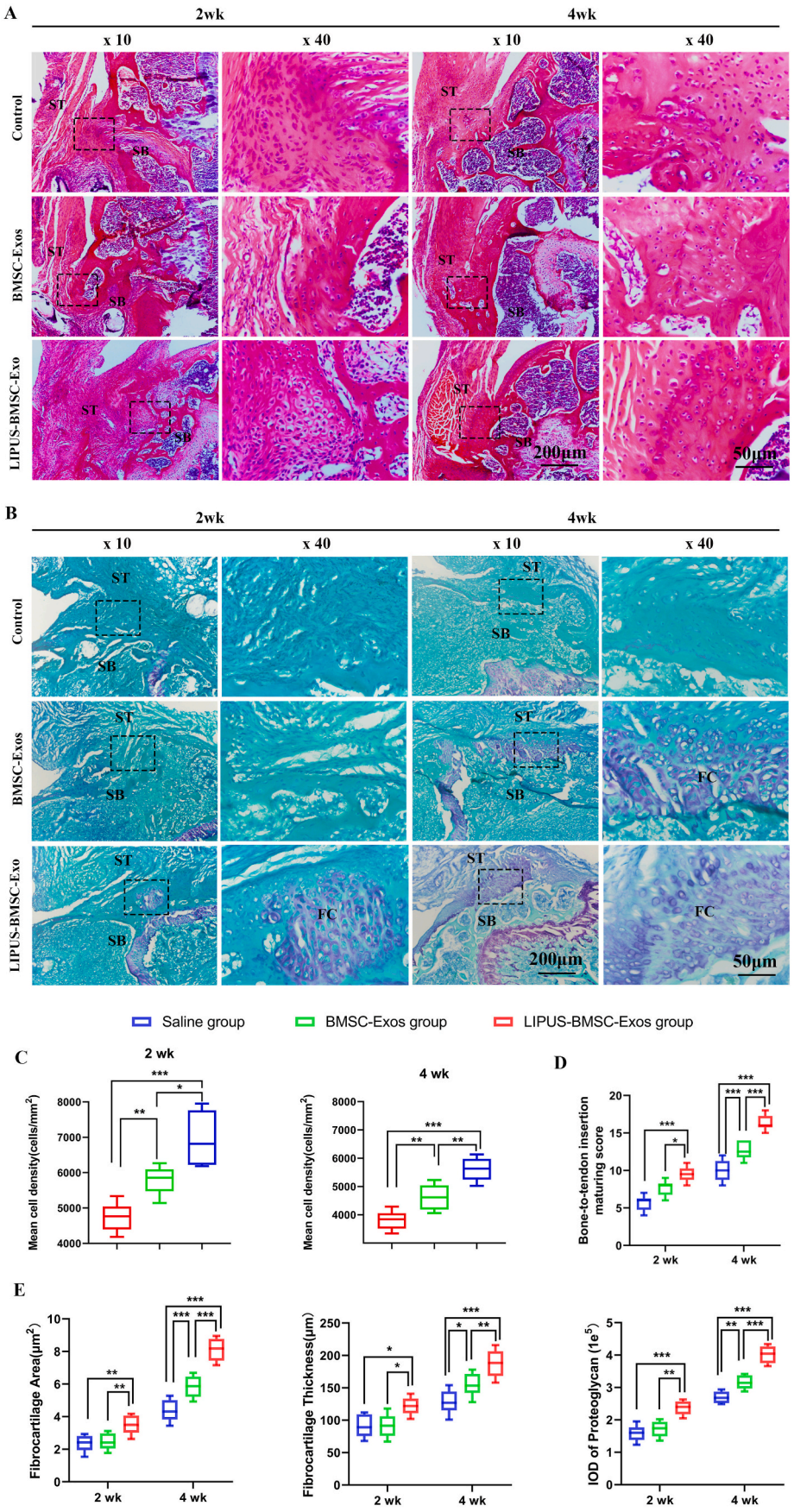

(caption on next page)

Fig. 3. LIPUS-BMSC-Exos enhance BTI healing by promoting regeneration of fibrocartilage zone (A) Representative hematoxylin and eosin stain images of BTI at weeks 2, and 4 postoperatively. The regions marked by dashed line in the × 10 pictures are amplified in corresponding 40 × pictures. Scale bars indicate 200 μm for × 10 and 50 μm for × 40. **(B)** Representative Toluidine blue/fast green images of BTI at weeks 2 and 4 postoperatively. The regions marked by dashed line in the × 10 pictures are amplified in corresponding × 40 pictures. Scale bars indicate 200 μm for × 10 and 50 μm for × 40. **(C)** Comparison of the mean cell density of BTI, **(D)** modified bone-to-tendon maturing score and **(E)** the area, thickness of the newly formed fibrocartilage layer and the integrated optical density (IOD) of proteoglycan among the 3 groups at postoperative 2 and 4 weeks. Values are presented as mean ± SD. n = 6 per group. $^{*}P < 0.05$, $^{**}P < 0.01$, $^{***}P < 0.001$. SB, subchondral bone; ST, supraspinatus tendon; BMSC-Exos, bone marrow mesenchymal stem cell-derived exosomes; LIPUS-BMSC-Exos, bone marrow mesenchymal stem cell-derived exosomes induced by LIPUS.

related genes compared with the Blank group ($P > 0.01$ for all, Fig. 7B-E).

3.9. LIPUS-BMSC-Exos inhibit adipogenetic differentiation of BMSCs

Recipient cells incubated with different Exos components showed varying degrees of ORO staining range and intensity (Fig. 8A). Quantitatively, the LIPUS-BMSC-Exos group showed less intensity of ORO staining and expression of adipogenesis-related genes (*Adipo*, *Retn* and *Pparg*) than those incubated with BMSC-Exos or blank liposomes ($P < 0.001$ for all, Fig. 8B-E). Meanwhile, BMSC-Exos also exhibited significantly lower level of ORO intensity and adipogenesis-related genes expression than the blank group ($P < 0.01$ for all, Fig. 8B-E).

3.10. miR-140 in LIPUS-BMSC-Exos promotes chondrogenesis and inhibit adipogenesis of BMSCs

To explore the functional mechanism of the enriched miRNAs during chondrogenesis and adipogenesis of BMSCs, the most abundant miRNA in LIPUS-BMSC-Exos, miR-140, was chosen as a potential target for further investigation. To fully unveil the underlying function of miR-140 in mediating chondrogenesis, a specific miR-140 mimic/inhibitor was transfected into native BMSCs. When miR-140 was overexpressed by transfecting the mimic, the Bern score and chondrogenic genes expression (*Sox9*, *Aggrecan*, and *Col2a1*) were evidently upregulated ($P < 0.001$ for all), nearly replicating the chondrogenic effect of LIPUS-BMSC-Exos (Fig. 7B-E). Whereas, the intensity of ORO and expression of adipogenesis-related genes (*Adipo*, *Retn* and *Pparg*) were significantly down-regulated in the miR-140 mimic group ($P < 0.001$ for all, Fig. 8B-E). On the other hand, when the elevated level of miR-140 conferred by LIPUS-BMSC-Exos was reversed by transfecting the miR-140 inhibitor, the expression of chondrogenic genes decreased significantly and expression of adipogenesis-related genes increased significantly compared with that of cells incubated with LIPUS-BMSC-Exos only ($P < 0.001$ for all, Fig. 7B-E, Fig. 8B-E). However, the miR-140 inhibitor group still showed significantly higher Bern score and chondrogenic genes expression, and significantly lower ORO intensity and adipogenesis-related genes expression ($P < 0.001$ for all, Fig. 7B-E, Fig. 8B-E). These results together suggest that miR-140 was the major contributor to LIPUS-BMSC-Exos-mediated chondrogenesis of BMSCs.

4. Discussion

In the present study, the feasibility of applying LIPUS-BMSC-Exos to promote fibrocartilage regeneration, alleviate fatty infiltration and induce chondrogenesis of BMSCs was evaluated. We found that LIPUS-BMSC-Exos, the nanocarriers secreted by BMSCs which were preconditioned by LIPUS, could effectively promote BTI healing through enhancing fibrocartilage regeneration and reducing rotator cuff fatty infiltration. We also showed that LIPUS-BMSC-Exos promoted chondrogenetic differentiation and inhibit adipogenetic differentiation of native BMSCs *in vitro*. Moreover, we demonstrated that miR-140, a potently pro-chondrogenic miRNA, was extremely highly enriched in LIPUS-BMSC-Exos. To sum up, we showed that LIPUS-BMSC-Exos could promote the shift from adipogenic to chondrogenic differentiation of BMSCs via delivering miR-140, thus enhancing BTI fibrocartilage regeneration and ameliorate rotator cuff fatty infiltration.

Over the past years, the application of MSCs for cartilage tissue repair and regeneration has received considerable attention [65–67]. In recent years, an increasing number of studies have reported that the paracrine actions are the main mechanism by which MSCs exert their therapeutic effects [68,69]. Exos, recently identified as important paracrine factors that mediate the intercellular communication, are critical effectors of MSCs [69–73]. It has been demonstrated that Exos can transfer proteins, RNA and other bioactive compounds into target cells and create an optimal microenvironment for maintaining cellular dynamic homeostasis, thus completing the transmission of biological information [74,75]. Due to specific advantages such as high stability, low immunogenicity, non-tumorigenicity and non-vascular thrombosis [74,76], MSCs-Exos therapy has been receiving increasing attention for tissue regeneration.

As for cartilage regeneration, the role of native MSCs-derived Exos for chondrogenesis is indefinable. Liu et al. [31] developed an in situ formed acellular hydrogel glue tissue patch combining Exos derived from human induced pluripotent stem cell derived MSCs (hiPSC-MSCs-Exos) for cartilage defect repair and found that the patch can retain hiPSC-MSCs-Exos and positively regulate both chondrocytes and BMSCs *in vitro* and promote cartilage defect repair *in vivo*. In view of the effect of in situ hydrogel glue in the study, there is no valid evidence to indicate MSCs-Exos can effectively induce chondrogenesis alone. Jing et al. [28] demonstrated that small extracellular vesicles (sEVs) derived from native human umbilical cord mesenchymal stem cells (hUCMSCs) do not generate obvious pro-chondrogenesis effects both *in vitro* and *in vivo*. However, Zhang et al. [30] demonstrated the efficacy of human embryonic MSCs-derived Exos in promoting cartilage regeneration, and the utility of MSCs Exos as a ready-to-use and "cell-free" therapeutic alternative to cell-based MSCs therapy *in vivo*. As for BTI healing, Wang et al. [52] showed that adipose stem cell-derived Exos can decrease fatty infiltration and enhance BTI healing *in vivo*. In accordance with Wang et al. [52] research, the present study revealed improved BTI healing by BMSC-Exos treatment which can be judged by the decrease of fibrous scar tissue formation, augment of fibrocartilaginous enthesis regeneration and better biomechanical properties. Meanwhile, although significant suppression of adipogenesis of native BMSCs were determined by BMSC-Exos, we did not find obvious pro-chondrogenesis effect of BMSC-Exos *in vitro*, which was inconsistent with Jing et al. [28] results. Actually, the results of *in vivo* and *in vitro* are not contradictory in the present study. The enhanced BTI healing in the BMSC-Exos group may be ascribed to two aspects. On the one hand, the anti-inflammatory effects of BMSC-Exos might effectively reduce the infiltration of inflammatory cells into the BTI interface, which can decrease the formation of fibrous scar tissue and enhance the regeneration of the normal tendon-bone insertion site [51,77]. On the other hand, the angiogenesis effects of BMSC-Exos can provide sufficient vascular invasion around the BTI junction, which is essential for promoting BTI healing and possibly contributes to aggregation and chondrogenesis of local stem cells after rotator cuff repair [29]. Combined with these results, we can draw conclusions carefully that BMSC-Exos may not possess obvious chondrogenetic effect alone,but they can still exhibit a degree of facilitating effect on fibrocartilage regeneration and BTI healing *in vivo* by promoting angiogenesis, decreasing infiltration of inflammatory cells and alleviating adipogenesis of native BMSCs.

Over the last two decades, LIPUS therapy has been proved to be an effective strategy to stimulate tendon-bone junction healing [35–43]. In

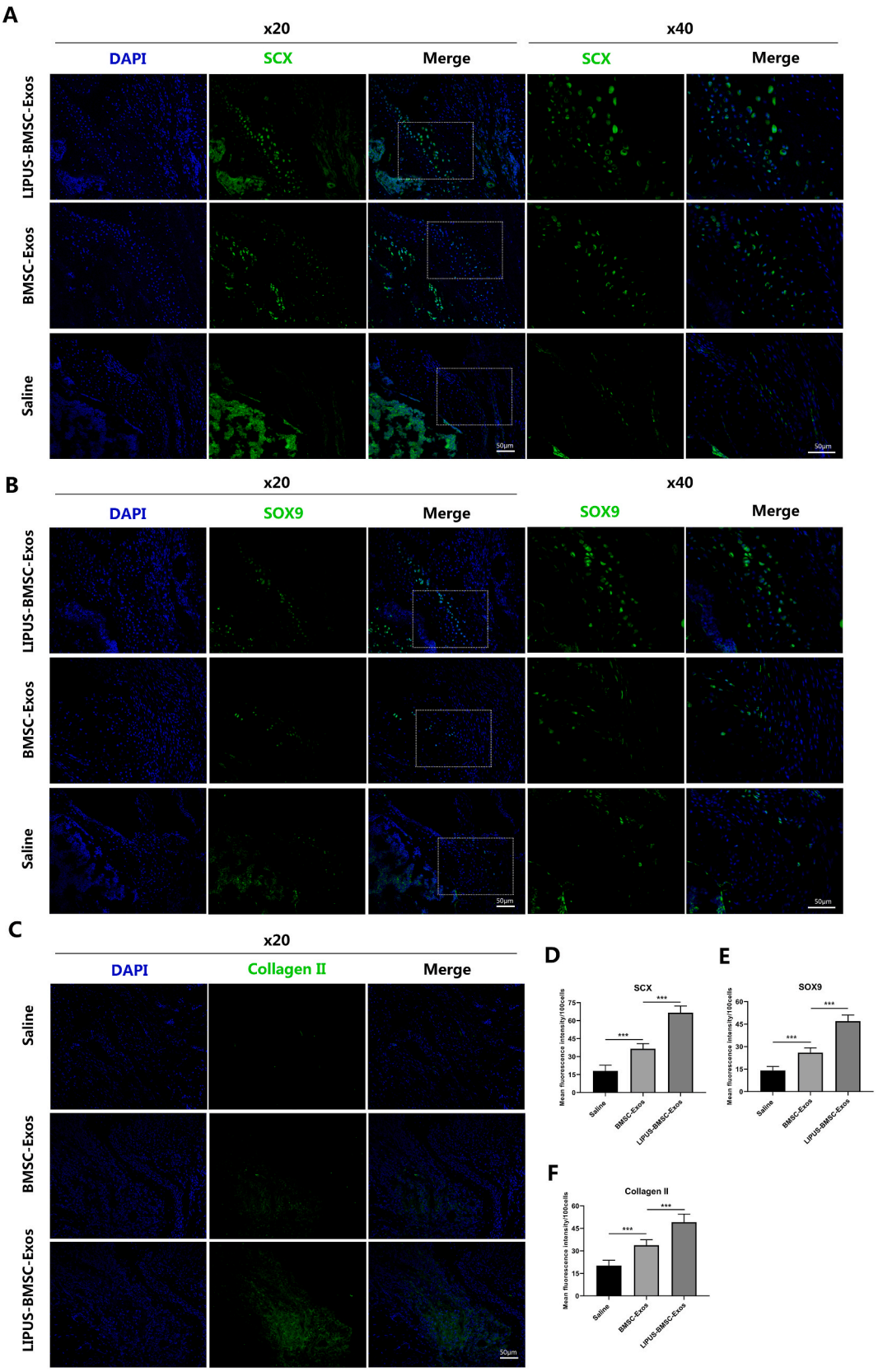

Fig. 4. LIPUS-BMSC-Exos promote expression of SCX, SOX9 and Collagen II at bone tendon interface. (A), (B), (C) Immunofluorescence staining of SCX, SOX9 and Collagen II in bone tendon interface, images in the first columns show nuclear staining with DAPI; the images in the second column show expression of the specific proteins while the images in the third column show overlay of proteins with DAPI. The last two columns of figure A and B show local zoom of the regions marked by dashed line in the third column. **(D), (E), (F)** Quantification of the expression proteins normalized to 100 cells. Values are presented as mean ± SD. n = 6 per group. ***$P < 0.001$.

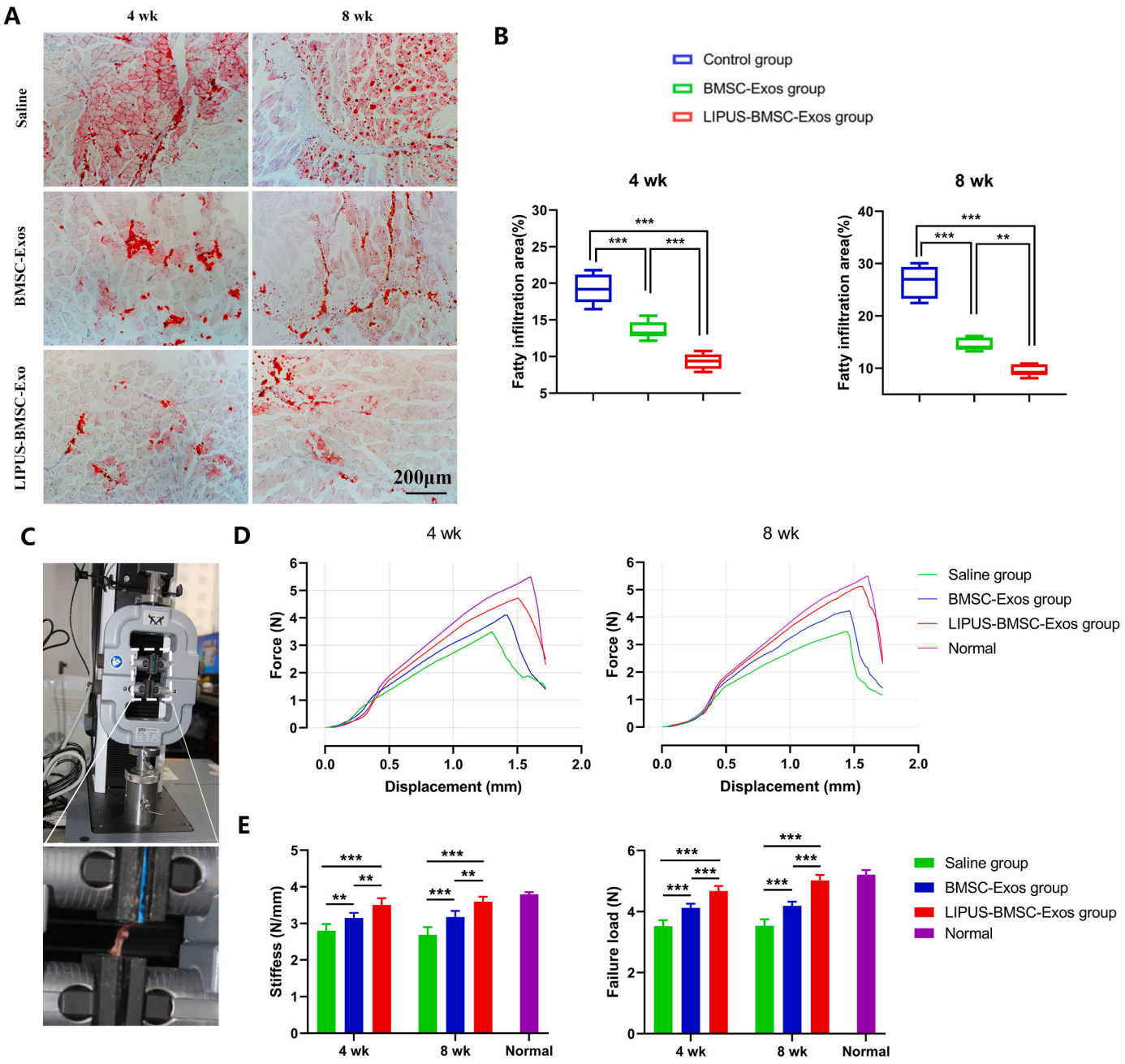

Fig. 5. LIPUS-BMSC-Exos decrease supraspinatus fatty infiltration and enhance biomechanical properties of the repaired rotator cuff. (A) Representative photomicrographs of the supraspinatus muscle stained with Oil Red O at postoperative 4 and 8 weeks. Scale bar = 200 μm. **(B)** Comparison of the fatty infiltration area of supraspinatus among the 3 groups at postoperative 4 and 8 weeks. Values are presented as mean ± SD. $^{**}P < 0.01$, $^{***}P < 0.001$. n = 6 per group. **(C)** Biomechanics testing of supraspinatus tendon humeral complex. **(D)** Representative force–displacement curves of supraspinatus tendon-humeral complex from normal shoulder and the three groups. **(E)** Comparison of the stiffness and failure load of supraspinatus tendon-humeral complex among the 3 groups at postoperative 4 and 8 weeks. Values are presented as mean ± SD. n = 6 per group. $^{**}P < 0.01$, $^{***}P < 0.001$. BMSC-Exos, bone marrow mesenchymal stem cell-derived exosomes; LIPUS-BMSC-Exos, bone marrow mesenchymal stem cell-derived exosomes induced by LIPUS.

these studies, a standard 30 mW/cm^2 intensity of LIPUS transcutaneous therapy *in vivo* turned out to enhance BTI healing through promoting angiogenesis, cartilage formation and maturation, endochondral bone formation and increasing the mechanical properties of the healing tissues of the tendon-bone junction [40,78]. LIPUS is also reported to enhance repair of articular cartilage in animal model of cartilage defect [79,80]. In a rabbit full-thickness osteochondral defects model, Cook et al. [80] demonstrated that daily low-intensity pulsed ultrasound has a significant positive effect on the healing of osteochondral defects. Meanwhile, LIPUS can induce chondrogenesis of BMSCs *in vitro* by enhancing the synthesis of matrix proteins such as collagen II and proteoglycans and expression of chondrogenic markers such as SOX9 and TIMP-2 [44]. Moreover, LIPUS preconditioning of BMSCs *in vitro* proved to be an effective cue to upregulate chondrogenic differentiation of native BMSCs *in vivo* [81].

As valid effect of LIPUS therapy for BTI healing has been confirmed and the fact that biological functions of the generated Exos were determined by the state of the donor cells, direct use of Exos derived from LIPUS preconditioned MSCs may represent a preferable and promising biotherapy agent for BTI regeneration. Hence, the present study construct Exos derived from BMSCs induced by LIPUS stimulation for fibrocartilage regeneration of BTI healing. We hypothesized that

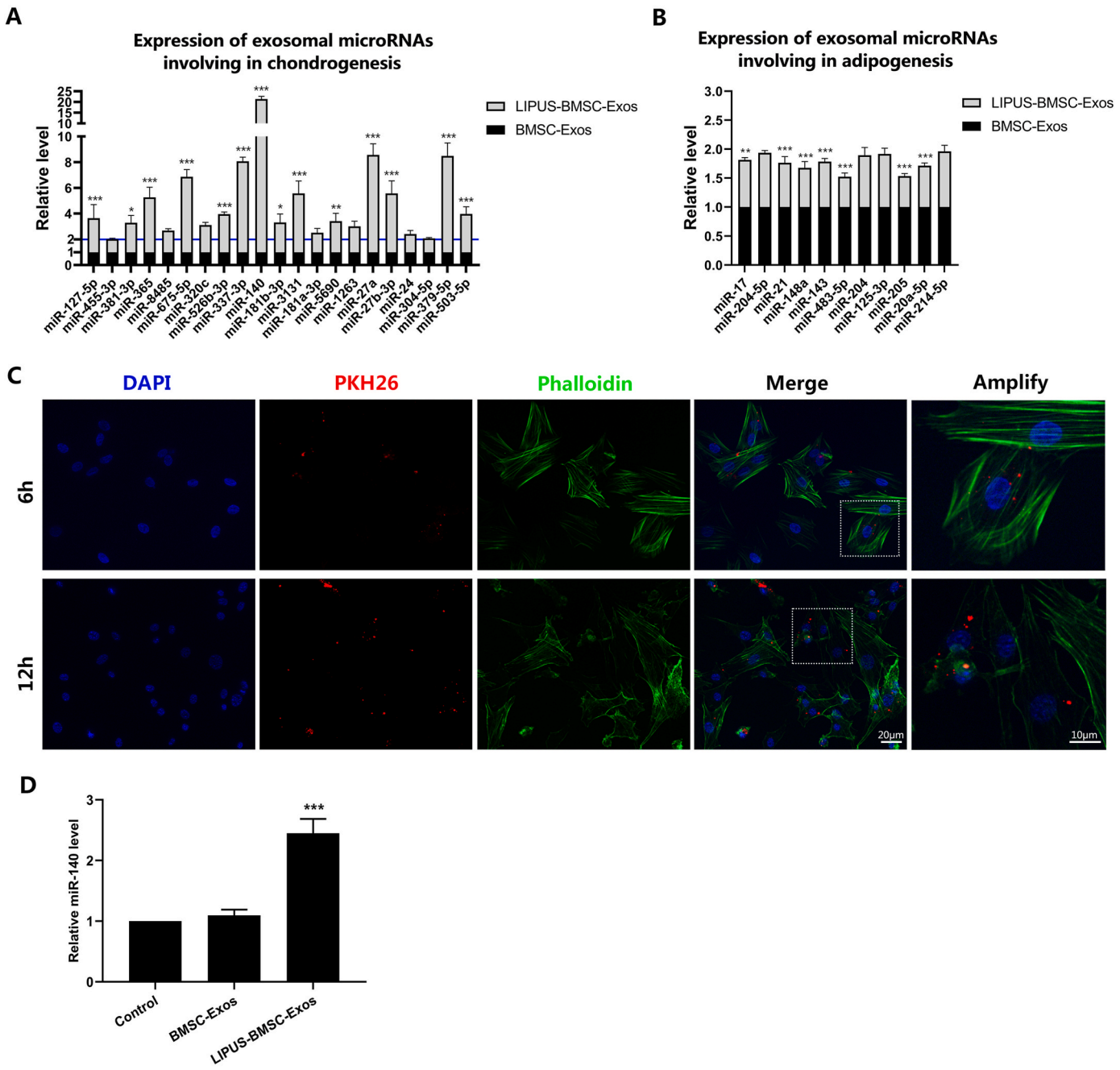

Fig. 6. LIPUS-BMSC-Exos transfer miR-140 into native BMSCs. (A), (B) qRT-PCR analysis of the enrichment of the chondrogenetic and adipogenetic miRNAs in LIPUS-BMSC-Exos compared with BMSC-Exos. n = 3 per group. **(C)** Representative fluorescence images of PKH26-labeled LIPUS-BMSC-Exos (red) uptake by BMSCs. Scale bar: 20 μm for the first 4 columns, 10 μm for the last column. **(D)** Detection of the level of miR-140 in BMSCs incubated with LIPUS-BMSC-Exos or BMSC-Exos for 12 h n = 3 per group. ***$P < 0.001$; **$P < 0.01$.

LIPUS preconditioning might impart BMSCs-derived Exos with chondrogenic potential to generate a valid chondrogenic microenvironment. As anticipated, the present results demonstrated that LIPUS-preconditioned BMSCs release Exos with potent chondrogenesis functions compared with BMSC-Exos both *in vivo* and *in vitro*. Meanwhile, as fatty infiltration of rotator cuff is the other factor that direct associated with unsatisfactory prognosis besides poor BTI healing, we also concern on the effect of LIPUS-BMSC-Exos on rotator cuff fatty infiltration and adipogenetic differentiation of MSCs. The present study showed that LIPUS-BMSC-Exos could effectively inhibit adipogenesis of native BMSCs and alleviate fatty infiltration of rotator cuff. The result threw light on the possible mechanism of shift from adipogenetic differentiation to chondrogenetic differentiation of BMSCs under the specific chondrogenic microenvironment cultivated by LIPUS-BMSC-Exos.

Exos-derived miRNAs, a class of small (20–24 nucleotide) non-coding RNAs, are one of the most important factors regulating the gene expression of recipient cells through translational repression [82]. Some studies even indicated that Exos mediate intercellular communication mainly through delivering miRNAs [83,84]. Furthermore, increasing evidence indicates that miRNAs from Exos cargoes are definitely involved in MSCs differentiation processes, such as angiogenesis, osteogenesis, adipogenesis and chondrogenesis [28,85–87]. To clarify the molecular mechanisms of LIPUS-BMSC-Exos on chondrocyte and adipocyte formation, we performed qRT-PCR to detect key miRNAs in LIPUS-BMSC-Exos. In the chondrogenesis-related miRNA profiles of LIPUS-BMSC-Exos, 14 of 21 (66.67 %) miRNAs were significantly

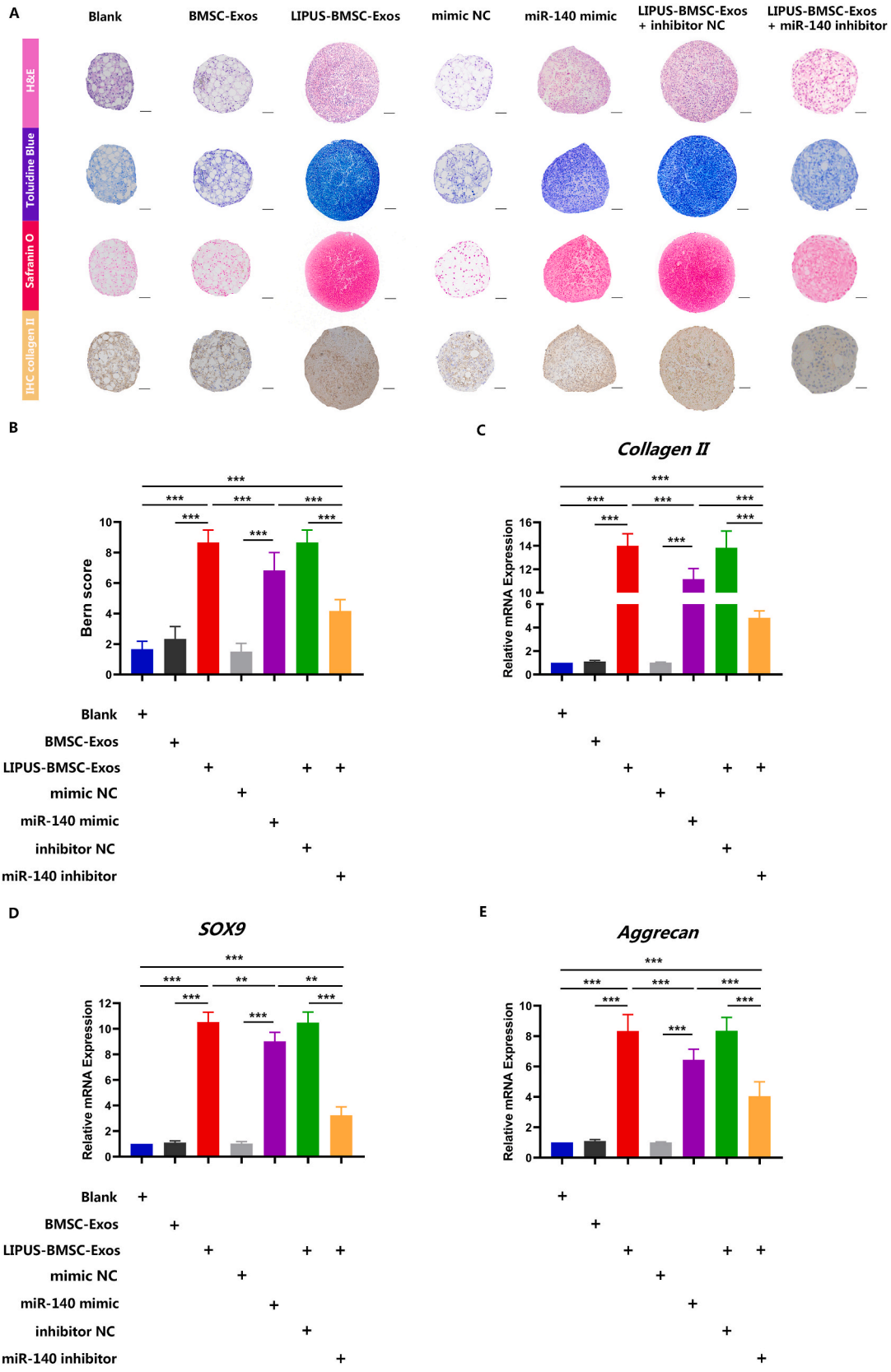

Fig. 7. Chondrogenesis of BMSCs induced by LIPUS-BMSC-Exos and miR-140 in LIPUS-BMSC-Exos. (A) Routine staining and immunohistochemical examinations after native BMSCs were incubated with different components and then subjected to pellet culture *in vitro*. Scale bar: 500 μm. **(B)** The total Bern score of different groups of histological examination. n = 6 per group. **(C), (D), (E)** The relative expressions of chondrogenesis-related genes (*Sox9*, *Aggrecan*, and *Col2a1*) determined by qRT-PCR after pellet culture *in vitro*. Values are presented as mean ± SD. n = 6 per group. ***$P < 0.001$; **$P < 0.01$.

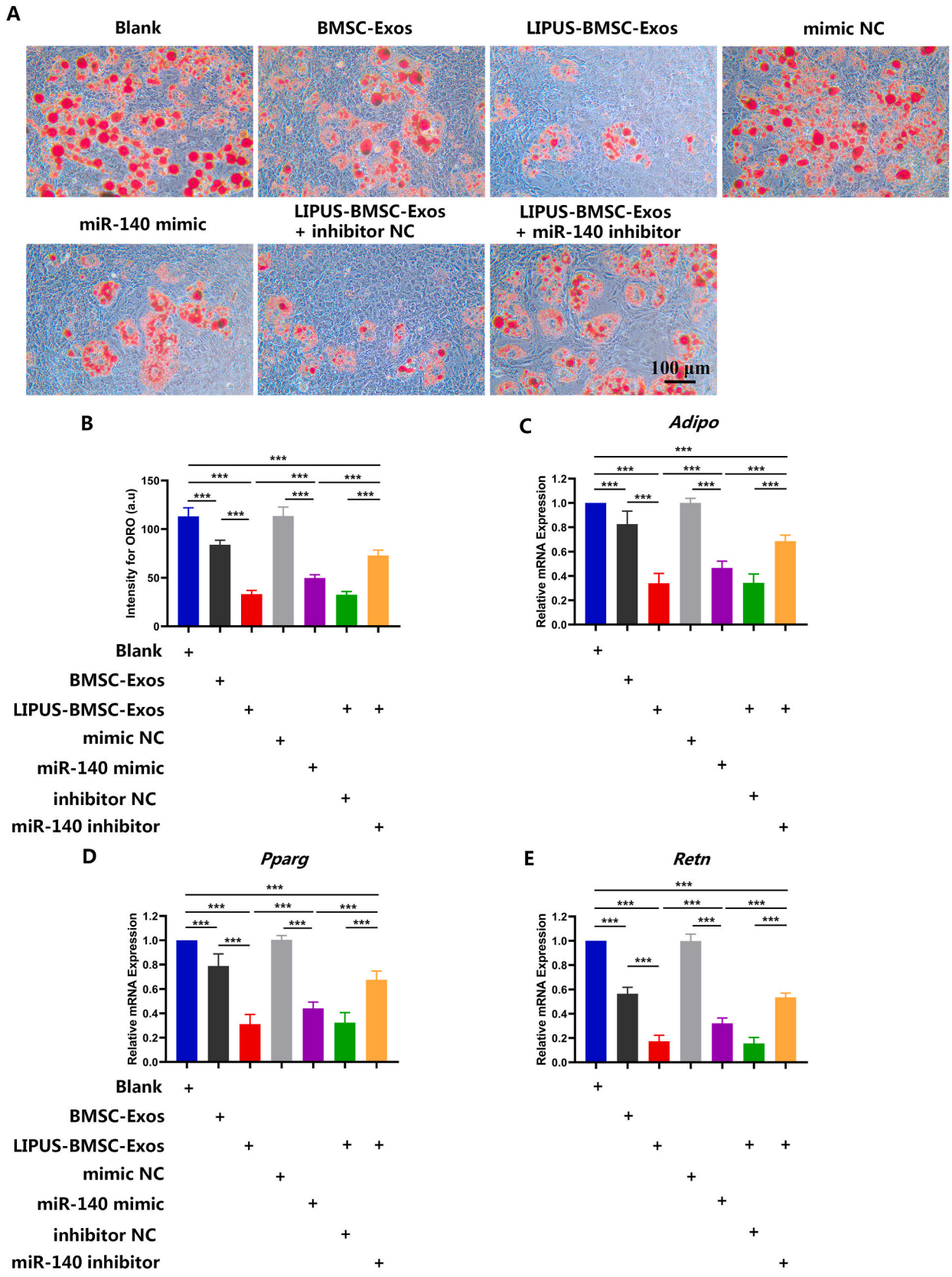

Fig. 8. LIPUS-BMSC-Exos inhibit adipogenic differentiation of BMSCs via delivering miR-140 (A) Representative ORO staining images of BMSCs treated with PBS, BMSC-Exos, LIPUS-BMSC-Exos, LIPUS-BMSC-Exos and a negative control of miR-140 mimic (mimic NC), miR-140 mimic, LIPUS-BMSC-Exos and a negative control of miR-140 inhibitor (inhibitor NC) and miR-140 inhibitor under adipogenic culture condition. Scale bar: 100 μm. **(B)** Quantification of the intensity for ORO staining in (A). n = 6 per group. **((C, D, E)** qRT-PCR analysis of the expression levels of Adipo, Retn and Pparg at day 7 of induction. Values are presented as mean ± SD. n = 6 per group. ***$P < 0.001$; **$P < 0.01$.

up-regulated compared to BMSC-Exos. At the same time, 7 of 11 (63.63 %) adipogenesis-related miRNAs were significantly down-regulated. It is reasonable to assume that LIPUS intervention remodel the miRNAs profiles of BMSCs-derived Exos and the highly enriched chondrogenesis-related miRNA cargoes in LIPUS-BMSC-Exos probably promote chondrogenesis of MSCs and fibrocartilage regeneration in BTI healing. Strikingly, miR-140, which has been reported to play an important role not only in the stability and maintenance of the cartilage matrix in chondrocytes but also promotes MSCs chondrogenesis [88], was found to be the most abundant miRNA in LIPUS-BMSC-Exos in the present study. The *in vitro* experiment revealed that over expression of miR-140 in BMSCs by miR-140 mimic replicate most of the chondrogenic effect of LIPUS-BMSC-Exos, whereas knockdown of miR-140 abolished most of pro-chondrogenic potential of LIPUS-BMSC-Exos, suggesting that miR-140 is one of the critical molecules in LIPUS-BMSC-Exos for stimulating cartilage formation. Interestingly, over expression of miR-140 could suppress adipogenesis of BMSCs. At the same time, most of anti-adipogenesis efficacy by LIPUS-BMSC-Exos could be abolished by miR-140 inhibitor, implying LIPUS treated BMSCs-Exos could possibly trigger the stable lineage-specific chondrogenic differentiation other than adipogenetic differentiation of MSCs via transferring miR-140. miR-140 mimic group showed inferior chondrogenic effect on MSCs than LIPUS-BMSC-Exos group, the probable reason might lie in the fact that there are totally 13 chondrogenic-related miRNAs which were significantly up-regulated in LIPUS-BMSC-Exos besides miR-140. Whether these miRNAs play essential roles in chondrogenesis of MSCs induced by LIPUS-BMSC-Exos still remains inconclusive. The mechanism can also explain why miR-140 inhibitor could not totally reverse the chondrogenic effect of LIPUS-BMSC-Exos.

In addition to popular research on tendon-bone healing, more and more basic studies focused on muscle degeneration after rotator cuff repair [15–19,21–23]. At best, the current intervention measures can at most halt the progression of fat infiltration, but cannot reverse the situation [15,18–20]. Gerber et al. [89] reported that the RC repair operation didn't result in substantial reversal of muscular fatty degeneration in a in a prospective study. Since then, pathophysiology of rotator cuff fatty infiltration and new therapies to improve the treatment were investigated in animal models. Gumucio et al. [90] used a rat model of rotator cuff injury to detect changes in the contractile properties of muscle fibers and the molecular regulation of fatty degeneration. They reported a significantly increase of fibrogenic, adipogenic, and autophagocytic mRNA and miRNA expression, dramatic accumulation of macrophages at fat accumulation area and a reduction in muscle fiber force production [90]. Similar results have been validated in rabbit animal models [91–93]. Wu et al. [92] demonstrated that fat accumulation and fibrosis were significantly increased from 1 to 8 weeks post-repair in a rabbit model of chronic rotator cuff tear compared to native rotator cuff. Consistent with these findings, the present study found that intact reattachment of supraspinatus tendon is incapable of prevent fatty infiltration progression. Although the cellular and molecular progress of fatty infiltration is complex and not fully understood, investigations are underway to elucidate the mechanism and develop targeted treatments. Trudel et al. [94] confirmed that adipocyte hyperplasia from distal part of the muscles was the main contributor to fat accumulation in the detached supraspinatus tendon. Kuwahara et al. [91] indicated that the initiation of adipogenic transcription factor (PPARγ and C/EBPα) expression result in failure to reverse the muscle fat infiltration after supraspinatus reattachment. Based on these studies, the present study focused on stem cell differentiation and we proved that the shift from adipogenic to chondrogenic differentiation of stem cells may be an important cue for halting adipocyte hyperplasia at the affected muscles. Therefore, attempts to inhibit resident stem cell or fibro-adipogenic progenitors [24] differentiate into adipocytes might contribute to create new management techniques that will halt or reverse the progression of fatty infiltration after rotator cuff repair.

Our findings broaden the understanding of the regenerative potential of LIPUS-treated-Exos on chondrogenesis of MSCs, and suggest the application of LIPUS-BMSC-Exos as an off-the-shelf bio-tool for inducing the stable differentiation of MSCs, enhancing BTI healing and ameliorate fatty infiltration of the rotator cuff. In contrast to cumbersome post-operative LIPUS therapy or expensive inducing hormonal cocktails preconditioning which containing transforming growth factor β (TGF-β), insulin-like growth factor (IGF), dexamethasone, insulin, transferrin, selenium, and ascorbic acid [95], a local injection of LIPUS preconditioned MSCs-derived Exos during operation is absolutely economical, simple, and convenient. Moreover, contrast to classical MSCs-derived Exos therapy, the LIPUS preconditioned MSCs-derived Exos demonstrated substantially superior pro-chondrogenesis efficacy on BTI fibrocartilage regeneration and also better anti-adipogenesis effect on preventing supraspinatus fatty infiltration.

This study has some limitations. First, although we continued to observe the generation of fibrocartilage tissue at the BTI junction which proved to be the most difficult part to regenerate, the biological and biomechanical properties of BTI junction are also determined by the other two zones of BTI, namely the subchondral bone and the tendon. It is still unclear whether LIPUS-BMSC-Exos can make a significant difference on the endochondral calcification, ossification, tendon collagen fiber formation, peritendinous fibrosis and tendon adhesion processes. Therefore, further research of the repairing effect on bone and tendon part could contribute to fully elucidate the regeneration potential of LIPUS-BMSC-Exos. Second, in many cases, LIPUS treatment entails 20 min of daily stimulation at intensity of 30 mW/cm^2, with a frequency of 1.5 MHz in pulsed-wave mode (200 μs burst sine waves repeated at 1.0 kHz) [43,47,48,51]. Most studies, including this one, have only studied a single LIPUS dose. Different dosages or use of different LIPUS stimulation parameters may reveal different effects of LIPUS on MSCs-Exos components and function, thus leading to different outcomes of rotator cuff healing in this specific model. Third, it is noteworthy that inhibition of miR-140 did not thoroughly block the beneficial effects of LIPUS-BMSC-Exos on chondrogenetic differentiation *in vitro*, indicating the implication of other miRNAs or other contents of exosomes, including proteins, lipids, glycoconjugates and other nucleic acids, might influence the regulatory effects of the LIPUS-BMSC-Exos through some unknown mechanisms. Meanwhile, Thomopoulos et al. [96] demonstrated that Hedgehog signaling within developing enthesis fibrocartilage cells is required for enthesis formation, whether the unique population of Hedgehog-responsive cells plays a role in fibrocartilage regeneration after BTI injury is unknown. Furthermore, although there are many advantages of mice as a model for acute supraspinatus tendon injury repair [45], mice are quadrupedal animals and joint motion and loading on the healing site are difficult to control owing to the inability to reliably immobilize the extremity or restrict weight bearing [53]. As mechanical loading is critical to the processes of fibrocartilage formation, mineral accumulation and collagen metabolism that are closely involved in a healing enthesis, it is not suitable to simply translate our findings into rotator cuff tear repair in humans. Finally, the pathophysiological process of the acute rotator cuff injury model is different from that of chronic rotator cuff injury, and the role of LIPUS-BMSC-Exos in chronic rotator cuff injury is unclear and needs further exploration.

In conclusion, our results demonstrated that Exos derived from LIPUS-preconditioned BMSCs are able to promote BTI fibrocartilage regeneration and ameliorate supraspinatus fatty infiltration in a murine rotator cuff repair model. The potential mechanism may be the positive regulation of pro-chondrogenetic and anti-adipogenetic of MSCs differentiation primarily through delivering miR-140. LIPUS-BMSC-Exos may become an innovative "Exos based strategy" for inducing chondrogenic differentiation of native MSCs, thereby proposing a new therapeutic method for BTI regeneration and rotator cuff healing in the near future.

Ethics approval and consent to participate

All the experimental procedures were performed with the approval of the Animal Committee of Xiangya Hospital of Central South University (No. 2019030490) and followed the guidelines of the Institutional Animal Care and Use Committee.

Funding

This work was supported by the National Natural Science Foundation of China (No.81730068, 82230085 , 82272572), the Research and Development Program in Key Areas of Hunan Province (NO. 2020SK2077) and the Science and Technology Major Project of Changsha (No. kh2102015).

Author contribution

Bing Wu, Hongbin Lu, Jianzhong Hu contributed to the study conception and design. Bing Wu performed the experiments. Huabin Chen helped with the animal experiments. Xin Shi, Changbiao Guan helped with the biochemical, cell and molecular biology experiments. Bing Wu, Tao Zhang analyzed the data and prepared all the figures. Bing Wu, Hongbin Lu drafted the manuscript. All authors reviewed and approved the manuscript.

Competing interests

The authors declare no competing interests. No benefits in any form have been or will be received from a commercial party related directly or indirectly to the subject of this manuscript.

Declaration of competing interest

The authors declare that they have no conflict of interests in this manuscript. No benefits in any form have been or will be received from a commercial party related directly or indirectly to the subject of this manuscript.

Abbreviations

MSCs	marrow mesenchymal stromal cells
BMSCs	bone marrow mesenchymal stromal cells
Exos	exosomes
LIPUS	low-intensity pulsed ultrasound stimulation
BTI	bone-tendon insertion
LIPUS-BMSC-Exos	Exos derived from LIPUS-preconditioned BMSCs
BMSC-Exos	Exos derived from un-preconditioned BMSCs
ST	supraspinatus tendon
STH	supraspinatus tendon-humeral
qRT-PCR	quantitative real-time polymerase chain reaction
FDA	food and the drug administration
ORO	Oil Red O
TEM	transmission electron microscope
NTA	nanoparticle tracking analysis
SMSTH	supraspinatus muscle-supraspinatus tendon-humeral
SM	supraspinatus muscle
EDTA	ethylene diamine tetraacetic acid
H&E	hematoxylin and eosin
SDS-PAGE	sodium dodecyl sulfate-polyacrylamide gel electrophoresis
Adipo	adiponectin
Retn	resistin
Pparg	peroxisome proliferator-activated receptor-gamma
SD	means ± standard deviation
ANOVA	one-way analysis of variance
MFI	mean fluorescence intensity
mimic NC	negative control of miR-140 mimic
inhibitor NC	negative control of miR-140 inhibitor
sEVs	small extracellular vesicles
hUCMSCs	human umbilical cord mesenchymal stem cells
TGF-β	transforming growth factor β
IGF	insulin-like growth factor

Appendix A. Supplementary data

Supplementary data to this article can be found online at https://doi.org/10.1016/j.jot.2024.07.009.

References

[1] Benjamin M, McGonagle D. Entheses: tendon and ligament attachment sites. Scand J Med Sci Sports 2009;19(4):520–7.
[2] Benjamin M, Toumi H, Ralphs JR, Bydder G, Best TM, Milz S. Where tendons and ligaments meet bone: attachment sites ('entheses') in relation to exercise and/or mechanical load. J Anat 2006;208(4):471–90.
[3] Leung KS, Chong WS, Chow DH, Zhang P, Cheung WH, Wong MW, et al. A comparative study on the biomechanical and histological properties of bone-to-bone, bone-to-tendon, and tendon-to-tendon healing: an achilles tendon-calcaneus model in goats. Am J Sports Med 2015;43(6):1413–21.
[4] Lu HH, Thomopoulos S. Functional attachment of soft tissues to bone: development, healing, and tissue engineering. Annu Rev Biomed Eng 2013;15:201–26.
[5] Jain NB, Higgins LD, Losina E, Collins J, Blazar PE, Katz JN. Epidemiology of musculoskeletal upper extremity ambulatory surgery in the United States. BMC Musculoskelet Disord 2014;15:4.
[6] Rodeo SA, Arnoczky SP, Torzilli PA, Hidaka C, Warren RF. Tendon-healing in a bone tunnel. A biomechanical and histological study in the dog. J Bone Joint Surg Am 1993;75(12):1795–803.
[7] Rossetti L, Kuntz LA, Kunold E, Schock J, Müller KW, Grabmayr H, et al. The microstructure and micromechanics of the tendon-bone insertion. Nat Mater 2017;16(6):664–70.
[8] Aoki M, Oguma H, Fukushima S, Ishii S, Ohtani S, Murakami G. Fibrous connection to bone after immediate repair of the canine infraspinatus: the most effective bony surface for tendon attachment. J Shoulder Elbow Surg 2001;10(2):123–8.
[9] Font Tellado S, Balmayor ER, Van Griensven M. Strategies to engineer tendon/ligament-to-bone interface: biomaterials, cells and growth factors. Adv Drug Deliv Rev 2015;94:126–40.
[10] Fujioka H, Thakur R, Wang GJ, Mizuno K, Balian G, Hurwitz SR. Comparison of surgically attached and non-attached repair of the rat Achilles tendon-bone interface. Cellular organization and type X collagen expression. Connect Tissue Res 1998;37(3–4):205–18.
[11] Mirzayan R, Weber AE, Petrigliano FA, Chahla J. Rationale for biologic augmentation of rotator cuff repairs. J Am Acad Orthop Surg 2019;27(13):468–78.
[12] Katthagen JC, Bucci G, Moatshe G, Tahal DS, Millett PJ. Improved outcomes with arthroscopic repair of partial-thickness rotator cuff tears: a systematic review. Knee Surg Sports Traumatol Arthrosc 2018;26(1):113–24.
[13] Chaudhury S, Dines JS, Delos D, Warren RF, Voigt C, Rodeo SA. Role of fatty infiltration in the pathophysiology and outcomes of rotator cuff tears. Arthritis Care Res 2012;64(1):76–82.
[14] Deniz G, Kose O, Tugay A, Guler F, Turan A. Fatty degeneration and atrophy of the rotator cuff muscles after arthroscopic repair: does it improve, halt or deteriorate? Arch Orthop Trauma Surg 2014;134(7):985–90.
[15] Goutallier D, Postel JM, Bernageau J, Lavau L, Voisin MC. Fatty muscle degeneration in cuff ruptures. Pre- and postoperative evaluation by CT scan. Clin Orthop Relat Res 1994;(304):78–83.
[16] Melis B, Nemoz C, Walch G. Muscle fatty infiltration in rotator cuff tears: descriptive analysis of 1688 cases. Orthop Traumatol Surg Res 2009;95(5):319–24.
[17] Melis B, Wall B, Walch G. Natural history of infraspinatus fatty infiltration in rotator cuff tears. J Shoulder Elbow Surg 2010;19(5):757–63.
[18] Goutallier D, Postel JM, Gleyze P, Leguilloux P, Van Driessche S. Influence of cuff muscle fatty degeneration on anatomic and functional outcomes after simple suture of full-thickness tears. J Shoulder Elbow Surg 2003;12(6):550–4.
[19] Gladstone JN, Bishop JY, Lo IK, Flatow EL. Fatty infiltration and atrophy of the rotator cuff do not improve after rotator cuff repair and correlate with poor functional outcome. Am J Sports Med 2007;35(5):719–28.
[20] Thomazeau H, Boukobza E, Morcet N, Chaperon J, Langlais F. Prediction of rotator cuff repair results by magnetic resonance imaging. Clin Orthop Relat Res 1997;344:275–83.
[21] Liem D, Lichtenberg S, Magosch P, Habermeyer P. Magnetic resonance imaging of arthroscopic supraspinatus tendon repair. J Bone Joint Surg Am 2007;89(8):1770–6.
[22] Kim SC, Shim SB, Kim WJ, Yoo JC. Preoperative rotator cuff tendon integrity, tear size, and muscle atrophy and fatty infiltration are associated with structural outcomes of arthroscopic revision rotator cuff repair. Knee Surg Sports Traumatol Arthrosc 2022;30(6):2029–38.
[23] Wang Z, Liu X, Davies MR, Horne D, Kim H, Feeley BT. A mouse model of delayed rotator cuff repair results in persistent muscle atrophy and fatty infiltration. Am J Sports Med 2018;46(12):2981–9.

[24] Agha O, Diaz A, Davies M, Kim HT, Liu X, Feeley BT. Rotator cuff tear degeneration and the role of fibro-adipogenic progenitors. Ann N Y Acad Sci 2021;1490(1):13–28.
[25] Kuzel BR, Grindel S, Papandrea R, Ziegler D. Fatty infiltration and rotator cuff atrophy. J Am Acad Orthop Surg 2013;21(10):613–23.
[26] Keshtkar S, Azarpira N, Ghahremani MH. Mesenchymal stem cell-derived extracellular vesicles: novel frontiers in regenerative medicine. Stem Cell Res Ther 2018;9(1):63.
[27] Narayanan K, Kumar S, Padmanabhan P, Gulyas B, Wan ACA, Rajendran VM. Lineage-specific exosomes could override extracellular matrix mediated human mesenchymal stem cell differentiation. Biomaterials 2018;182:312–22.
[28] Jing H, Zhang X, Luo K, Luo Q, Yin M, Wang W, et al. miR-381-abundant small extracellular vesicles derived from kartogenin-preconditioned mesenchymal stem cells promote chondrogenesis of MSCs by targeting TAOK1. Biomaterials 2020;231:119682.
[29] Huang Y, He B, Wang L, Yuan B, Shu H, Zhang F, et al. Bone marrow mesenchymal stem cell-derived exosomes promote rotator cuff tendon-bone healing by promoting angiogenesis and regulating M1 macrophages in rats. Stem Cell Res Ther 2020;11(1):496.
[30] Zhang S, Chu WC, Lai RC, Lim SK, Hui JH, Toh WS. Exosomes derived from human embryonic mesenchymal stem cells promote osteochondral regeneration. Osteoarthritis Cartilage 2016;24(12):2135–40.
[31] Liu X, Yang Y, Li Y, Niu X, Zhao B, Wang Y, et al. Integration of stem cell-derived exosomes with in situ hydrogel glue as a promising tissue patch for articular cartilage regeneration. Nanoscale 2017;9(13):4430–8.
[32] Mao G, Zhang Z, Hu S, Zhang Z, Chang Z, Huang Z, et al. Exosomes derived from miR-92a-3p-overexpressing human mesenchymal stem cells enhance chondrogenesis and suppress cartilage degradation via targeting WNT5A. Stem Cell Res Ther 2018;9(1):247.
[33] Garcia NA, Ontoria-Oviedo I, González-King H, Diez-Juan A, Sepúlveda P. Glucose starvation in cardiomyocytes enhances exosome secretion and promotes angiogenesis in endothelial cells. PLoS One 2015;10(9):e0138849.
[34] Angle SR, Sena K, Sumner DR, Virdi AS. Osteogenic differentiation of rat bone marrow stromal cells by various intensities of low-intensity pulsed ultrasound. Ultrasonics 2011;51(3):281–8.
[35] Qin L, Lu H, Fok P, Cheung W, Zheng Y, Lee K, et al. Low-intensity pulsed ultrasound accelerates osteogenesis at bone-tendon healing junction. Ultrasound Med Biol 2006;32(12):1905–11.
[36] Lovric V, Ledger M, Goldberg J, Harper W, Bertollo N, Pelletier MH, et al. The effects of low-intensity pulsed ultrasound on tendon-bone healing in a transosseous-equivalent sheep rotator cuff model. Knee Surg Sports Traumatol Arthrosc 2013;21(2):466–75.
[37] Lu CC, Liu YC, Cheng YM, Chih TT, Tien YC. Augmentation of tendon-bone interface healing with low-intensity pulsed ultrasound. Orthopedics 2009;32(3):173.
[38] Lu H, Qin L, Fok P, Cheung W, Lee K, Guo X, et al. Low-intensity pulsed ultrasound accelerates bone-tendon junction healing: a partial patellectomy model in rabbits. Am J Sports Med 2006;34(8):1287–96.
[39] Lu H, Qin L, Cheung W, Lee K, Wong W, Leung K. Low-intensity pulsed ultrasound accelerated bone-tendon junction healing through regulation of vascular endothelial growth factor expression and cartilage formation. Ultrasound Med Biol 2008;34(8):1248–60.
[40] Lu MH, Zheng YP, Huang QH, Lu HB, Qin L. Low intensity pulsed ultrasound increases the mechanical properties of the healing tissues at bone-tendon junction. Annu Int Conf IEEE Eng Med Biol Soc 2009;2009:2141–4.
[41] Lu H, Chen C, Qu J, Chen H, Chen Y, Zheng C, et al. Initiation timing of low-intensity pulsed ultrasound stimulation for tendon-bone healing in a rabbit model. Am J Sports Med 2016;44(10):2706–15.
[42] Lu H, Liu F, Chen C, Wang Z, Chen H, Qu J, et al. Low-intensity pulsed ultrasound stimulation for tendon-bone healing: a dose-dependent study. Am J Phys Med Rehabil 2018;97(4):270–7.
[43] Chen C, Zhang T, Liu F, Qu J, Chen Y, Fan S, et al. Effect of low-intensity pulsed ultrasound after autologous adipose-derived stromal cell transplantation for bone-tendon healing in a rabbit model. Am J Sports Med 2019;47(4):942–53.
[44] Lee HJ, Choi BH, Min BH, Son YS, Park SR. Low-intensity ultrasound stimulation enhances chondrogenic differentiation in alginate culture of mesenchymal stem cells. Artif Organs 2006;30(9):707–15.
[45] Lebaschi AH, Deng XH, Camp CL, Zong J, Cong GT, Carballo CB, et al. Biomechanical, histologic, and molecular evaluation of tendon healing in a new murine model of rotator cuff repair. Arthroscopy 2018;34(4):1173–83.
[46] Zhang T, Chen Y, Chen C, Li S, Xiao H, Wang L, et al. Treadmill exercise facilitated rotator cuff healing is coupled with regulating periphery neuropeptides expression in a murine model. J Orthop Res 2021;39(3):680–92.
[47] Tang CH, Yang RS, Huang TH, Lu DY, Chuang WJ, Huang TF, et al. Ultrasound stimulates cyclooxygenase-2 expression and increases bone formation through integrin, focal adhesion kinase, phosphatidylinositol 3-kinase, and Akt pathway in osteoblasts. Mol Pharmacol 2006;69(6):2047–57.
[48] Hsu HC, Fong YC, Chang CS, Hsu CJ, Hsu SF, Lin JG, et al. Ultrasound induces cyclooxygenase-2 expression through integrin, integrin-linked kinase, Akt, NF-kappaB and p300 pathway in human chondrocytes. Cell Signal 2007;19(11):2317–28.
[49] Dong L, Pu Y, Zhang L, Qi Q, Xu L, Li W, et al. Human umbilical cord mesenchymal stem cell-derived extracellular vesicles promote lung adenocarcinoma growth by transferring miR-410. Cell Death Dis 2018;9(2):218.
[50] Bell R, Taub P, Cagle P, Flatow EL, Andarawis-Puri N. Development of a mouse model of supraspinatus tendon insertion site healing. J Orthop Res 2015;33(1):25–32.
[51] Li S, Xu Z, Wang Z, Xiang J, Zhang T, Lu H. Acceleration of bone-tendon interface healing by low-intensity pulsed ultrasound is mediated by macrophages. Phys Ther 2021;101(7):zab055.
[52] Wang C, Hu Q, Song W, Yu W, He Y. Adipose stem cell-derived exosomes decrease fatty infiltration and enhance rotator cuff healing in a rabbit model of chronic tears. Am J Sports Med 2020;48(6):1456–64.
[53] Wang D, Tan H, Lebaschi AH, Nakagawa Y, Wada S, Donnelly PE, et al. Kartogenin enhances collagen organization and mechanical strength of the repaired enthesis in a murine model of rotator cuff repair. Arthroscopy 2018;34(9):2579–87.
[54] Wang W, Chen HH, Yang XH, Xu G, Chan KM, Qin L. Postoperative programmed muscle tension augmented osteotendinous junction repair. Int J Sports Med 2007;28(8):691–6.
[55] Chow DH, Suen PK, Fu LH, Cheung WH, Leung KS, Wong MW, et al. Extracorporeal shockwave therapy for treatment of delayed tendon-bone insertion healing in a rabbit model: a dose-response study. Am J Sports Med 2012;40(12):2862–71.
[56] Ide J, Kikukawa K, Hirose J, Iyama K, Sakamoto H, Fujimoto T, et al. The effect of a local application of fibroblast growth factor-2 on tendon-to-bone remodeling in rats with acute injury and repair of the supraspinatus tendon. J Shoulder Elbow Surg 2009;18(3):391–8.
[57] Thankam FG, Chandra IS, Kovilam AN, Diaz CG, Volberding BT, Dilisio MF, et al. Amplification of mitochondrial activity in the healing response following rotator cuff tendon injury. Sci Rep 2018;8(1):17027.
[58] Mattucci SF, Cronin DS. A method to characterize average cervical spine ligament response based on raw data sets for implementation into injury biomechanics models. J Mech Behav Biomed Mater 2015;41:251–60.
[59] Hu Y, Xu R, Chen CY, Rao SS, Xia K, Huang J, et al. Extracellular vesicles from human umbilical cord blood ameliorate bone loss in senile osteoporotic mice. Metabolism 2019;95:93–101.
[60] Ti D, Hao H, Tong C, Liu J, Dong L, Zheng J, et al. LPS-preconditioned mesenchymal stromal cells modify macrophage polarization for resolution of chronic inflammation via exosome-shuttled let-7b. J Transl Med 2015;13:308.
[61] Grogan SP, Barbero A, Winkelmann V, Rieser F, Fitzsimmons JS, O'Driscoll S, et al. Visual histological grading system for the evaluation of in vitro-generated neocartilage. Tissue Eng 2006;12(8):2141–9.
[62] Della Bella E, Menzel U, Basoli V, Tourbier C, Alini M, Stoddart MJ. Differential regulation of circRNA, miRNA, and piRNA during early osteogenic and chondrogenic differentiation of human mesenchymal stromal cells. Cells 2020;9(2).
[63] Robert AW, Marcon BH, Dallagiovanna B, Shigunov P. Adipogenesis, osteogenesis, and chondrogenesis of human mesenchymal stem/stromal cells: a comparative transcriptome approach. Front Cell Dev Biol 2020;8:561.
[64] Sun H, Hu S, Zhang Z, Lun J, Liao W, Zhang Z. Expression of exosomal microRNAs during chondrogenic differentiation of human bone mesenchymal stem cells. J Cell Biochem 2019;120(1):171–81.
[65] Wang W, Li B, Li Y, Jiang Y, Ouyang H, Gao C. In vivo restoration of full-thickness cartilage defects by poly(lactide-co-glycolide) sponges filled with fibrin gel, bone marrow mesenchymal stem cells and DNA complexes. Biomaterials 2010;31(23):5953–65.
[66] Hashimoto Y, Nishida Y, Takahashi S, Nakamura H, Mera H, Kashiwa K, et al. Transplantation of autologous bone marrow-derived mesenchymal stem cells under arthroscopic surgery with microfracture versus microfracture alone for articular cartilage lesions in the knee: a multicenter prospective randomized control clinical trial. Regen Ther 2019;11:106–13.
[67] Sun Y, You Y, Jiang W, Zhai Z, Dai K. 3D-bioprinting a genetically inspired cartilage scaffold with GDF5-conjugated BMSC-laden hydrogel and polymer for cartilage repair. Theranostics 2019;9(23):6949–61.
[68] Lai RC, Yeo RW, Lim SK. Mesenchymal stem cell exosomes. Semin Cell Dev Biol 2015;40:82–8.
[69] Rani S, Ryan AE, Griffin MD, Ritter T. Mesenchymal stem cell-derived extracellular vesicles: toward cell-free therapeutic applications. Mol Ther 2015;23(5):812–23.
[70] Kim YG, Choi J, Kim K. Mesenchymal stem cell-derived exosomes for effective cartilage tissue repair and treatment of osteoarthritis. Biotechnol J 2020;15(12):e2000082.
[71] Mendt M, Rezvani K, Shpall E. Mesenchymal stem cell-derived exosomes for clinical use. Bone Marrow Transplant 2019;54(Suppl 2):789–92.
[72] Park KS, Bandeira E, Shelke GV, Lässer C, Lötvall J. Enhancement of therapeutic potential of mesenchymal stem cell-derived extracellular vesicles. Stem Cell Res Ther 2019;10(1):288.
[73] Vonk LA, van Dooremalen SFJ, Liv N, Klumperman J, Coffer PJ, Saris DBF, et al. Mesenchymal stromal/stem cell-derived extracellular vesicles promote human cartilage regeneration in vitro. Theranostics 2018;8(4):906–20.
[74] Pegtel DM, Gould SJ. Exosomes. Annu Rev Biochem 2019;88:487–514.
[75] Kalluri R, LeBleu VS. The biology, function, and biomedical applications of exosomes. Science 2020;367(6478).
[76] De Jong OG, Van Balkom BW, Schiffelers RM, Bouten CV, Verhaar MC. Extracellular vesicles: potential roles in regenerative medicine. Front Immunol 2014;5:608.
[77] Kawamura S, Ying L, Kim HJ, Dynybil C, Rodeo SA. Macrophages accumulate in the early phase of tendon-bone healing. J Orthop Res 2005;23(6):1425–32.
[78] Ying ZM, Lin T, Yan SG. Low-intensity pulsed ultrasound therapy: a potential strategy to stimulate tendon-bone junction healing. J Zhejiang Univ - Sci B 2012;13(12):955–63.

[79] Park SR, Park SH, Jang KW, Cho HS, Cui JH, An HJ, et al. The effect of sonication on simulated osteoarthritis. Part II: alleviation of osteoarthritis pathogenesis by 1 MHz ultrasound with simultaneous hyaluronate injection. Ultrasound Med Biol 2005;31(11):1559–66.
[80] Cook SD, Salkeld SL, Popich-Patron LS, Ryaby JP, Jones DG, Barrack RL. Improved cartilage repair after treatment with low-intensity pulsed ultrasound. Clin Orthop Relat Res 2001;(391 Suppl):S231–43.
[81] Cui JH, Park SR, Park K, Choi BH, Min BH. Preconditioning of mesenchymal stem cells with low-intensity ultrasound for cartilage formation in vivo. Tissue Eng 2007;13(2):351–60.
[82] Yu X, Odenthal M, Fries JW. Exosomes as miRNA carriers: formation-function-future. Int J Mol Sci 2016;17(12).
[83] Fleshner M, Crane CR. Exosomes, DAMPs and miRNA: features of stress physiology and immune homeostasis. Trends Immunol 2017;38(10):768–76.
[84] Mori MA, Ludwig RG, Garcia-Martin R, Brandão BB, Kahn CR. Extracellular miRNAs: from biomarkers to mediators of physiology and disease. Cell Metab. 2019;30(4):656–73.
[85] Olejarz W, Kubiak-Tomaszewska G, Chrzanowska A, Lorenc T. Exosomes in angiogenesis and anti-angiogenic therapy in cancers. Int J Mol Sci 2020;21(16).
[86] Zhu S, Yao F, Qiu H, Zhang G, Xu H, Xu J. Coupling factors and exosomal packaging microRNAs involved in the regulation of bone remodelling. Biol Rev Camb Philos Soc 2018;93(1):469–80.
[87] Lorente-Cebrián S, González-Muniesa P, Milagro FI, Martínez JA. MicroRNAs and other non-coding RNAs in adipose tissue and obesity: emerging roles as biomarkers and therapeutic targets. Clin Sci (Lond). 2019;133(1):23–40.
[88] Duan L, Liang Y, Xu X, Xiao Y, Wang D. Recent progress on the role of miR-140 in cartilage matrix remodelling and its implications for osteoarthritis treatment. Arthritis Res Ther 2020;22(1):194.
[89] Gerber C, Fuchs B, Hodler J. The results of repair of massive tears of the rotator cuff. J Bone Joint Surg Am 2000;82(4):505–15.
[90] Gumucio JP, Davis ME, Bradley JR, Stafford PL, Schiffman CJ, Lynch EB, et al. Rotator cuff tear reduces muscle fiber specific force production and induces macrophage accumulation and autophagy. J Orthop Res 2012;30(12):1963–70.
[91] Kuwahara Y, Kishimoto KN, Itoigawa Y, Okuno H, Hatta T, Matsuzawa G, et al. Fatty degeneration and wnt10b expression in the supraspinatus muscle after surgical repair of torn rotator cuff tendon. J Orthop Surg 2019;27(3):2309499019864817.
[92] Wu IT, Gibbons MC, Esparza MC, Vasquez-Bolanos LS, Hyman SA, Dorn SN, et al. The "second hit" of repair in a rabbit model of chronic rotator cuff tear. Front Physiol 2022;13:801829.
[93] Vargas-Vila MA, Gibbons MC, Wu IT, Esparza MC, Kato K, Johnson SD, et al. Progression of muscle loss and fat accumulation in a rabbit model of rotator cuff tear. J Orthop Res 2022;40(5):1016–25.
[94] Trudel G, Uhthoff HK, Wong K, Dupuis J, Laneuville O. Adipocyte hyperplasia: the primary mechanism of supraspinatus intramuscular fat accumulation after a complete rotator cuff tendon tear: a study in the rabbit. Adipocyte 2019;8(1):144–53.
[95] Liang Y, Idrees E, Szojka ARA, Andrews SHJ, Kunze M, Mulet-Sierra A, et al. Chondrogenic differentiation of synovial fluid mesenchymal stem cells on human meniscus-derived decellularized matrix requires exogenous growth factors. Acta Biomater 2018;80:131–43.
[96] Schwartz AG, Long F, Thomopoulos S. Enthesis fibrocartilage cells originate from a population of Hedgehog-responsive cells modulated by the loading environment. Development 2015;142(1):196–206.